Li-Ion Battery

Byungwoo Park

Department of Materials Science and Engineering
Seoul National University

http://bp.snu.ac.kr

Rechargeable Batteries

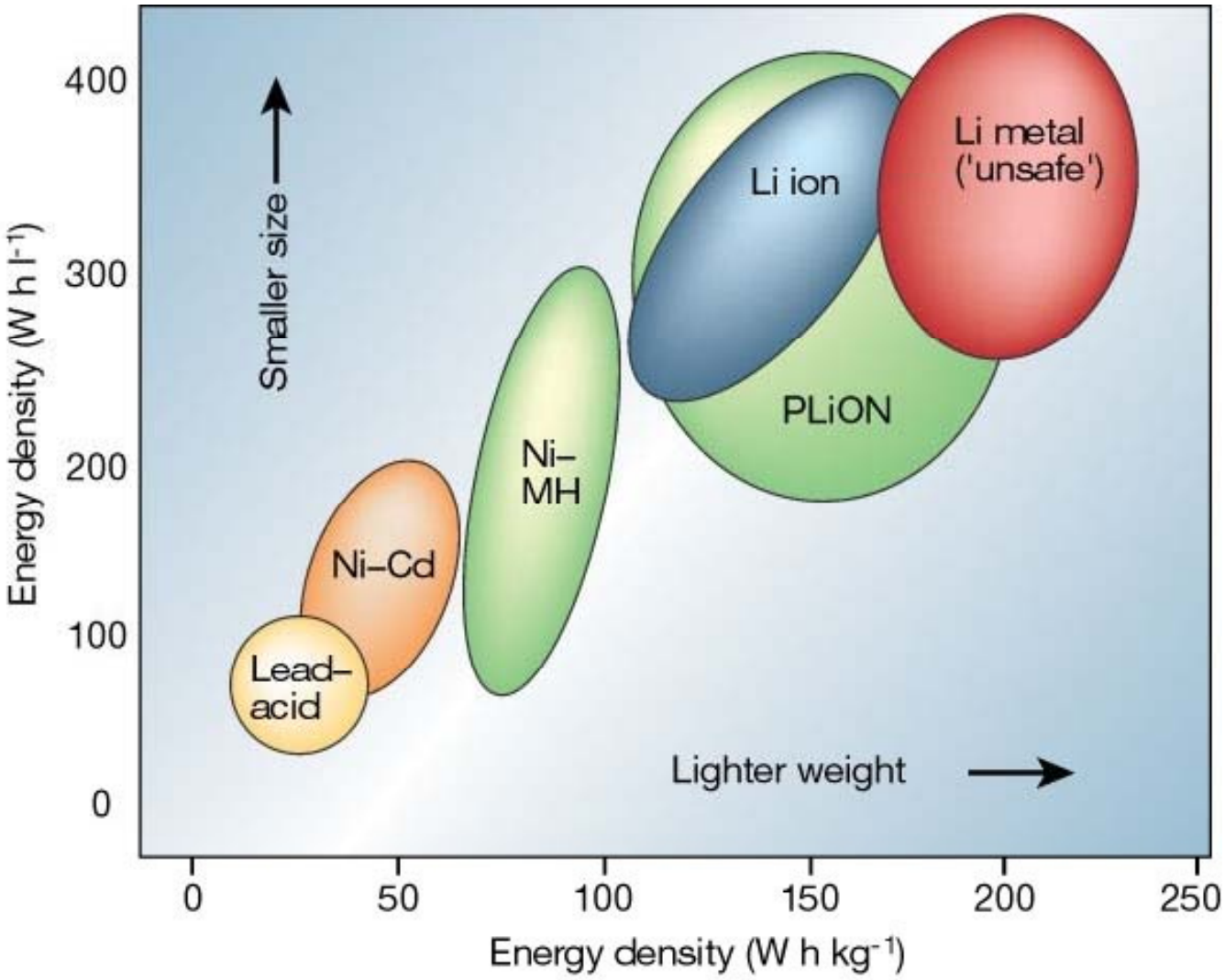

J.-M. Tarascon's group, *Nature* (2001)

Applications of Advanced Li-Ion Battery

PMP

Laptop Computer

Mobile Phone

MP3 Player

Portable Game

Digital Camera

High-Power Applications

Hybrid Electric Vehicles (HEV)

Toyota Prius HEV

Power Tools

Makita

E-Motorcycle

Greenwit

Electrode Materials

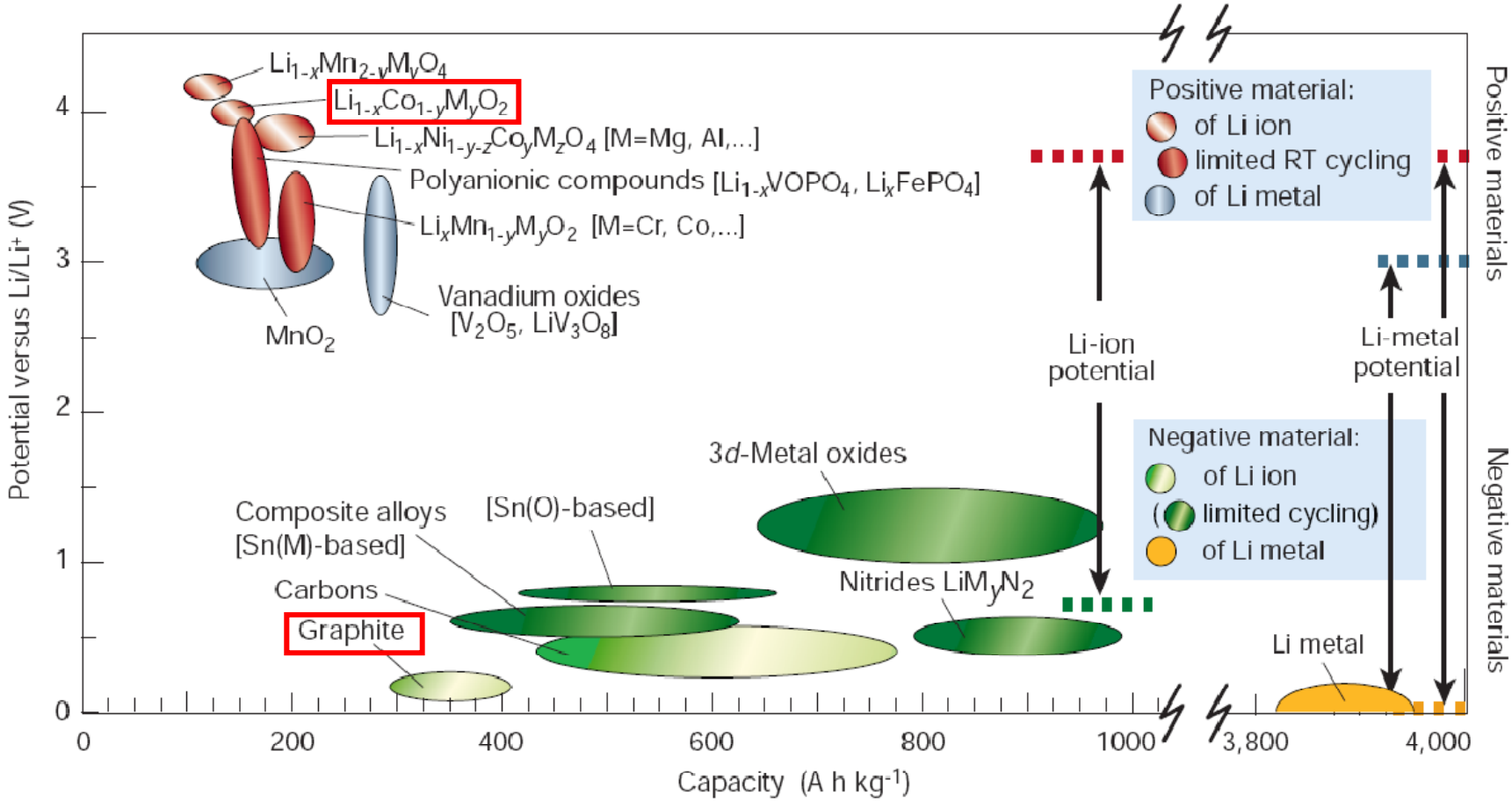

J.-M. Tarascon's group, *Nature* (2001)

Li-Ion Battery Mechanisms

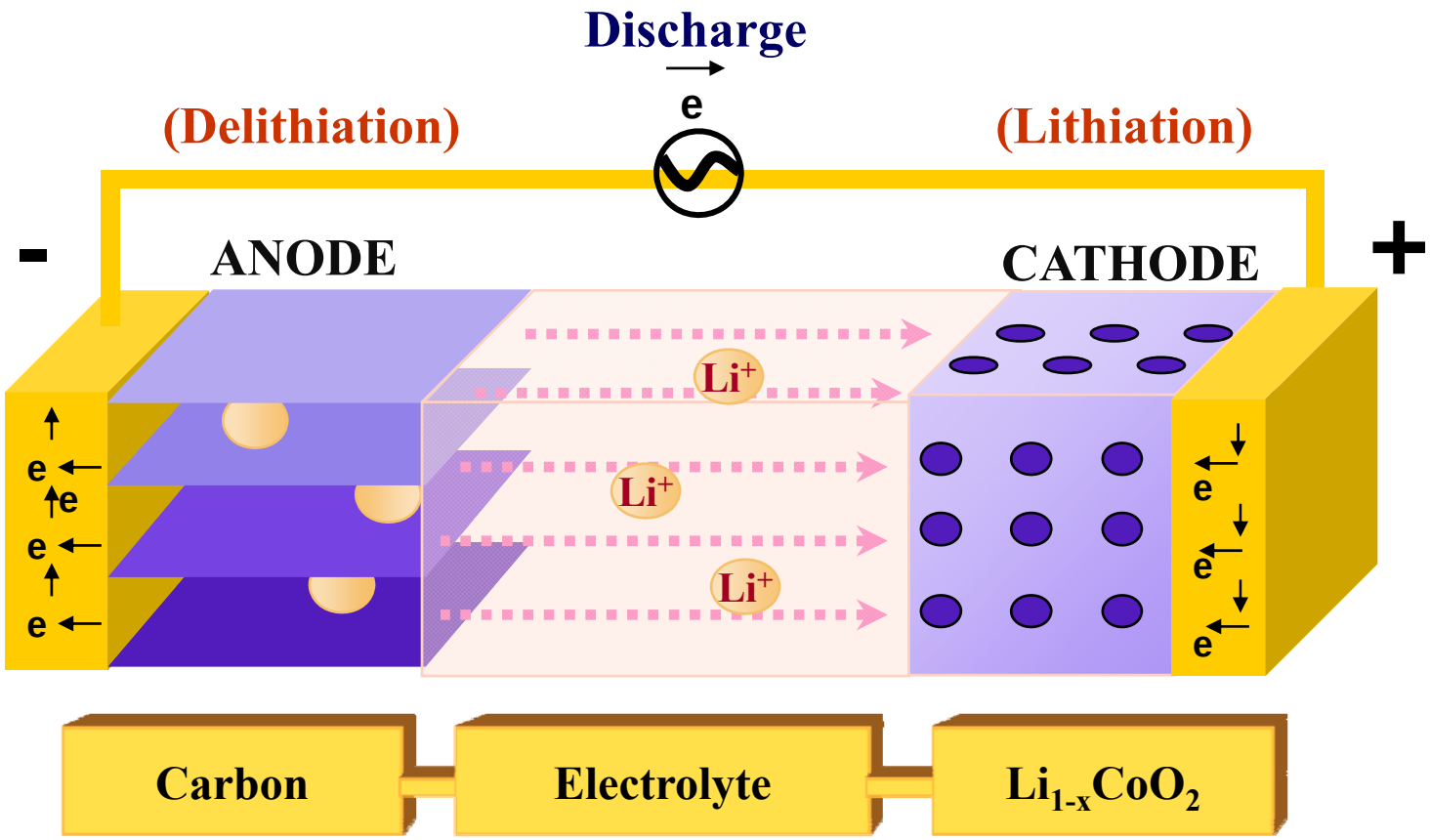

- Capacity
- Cycle Life
- Safety

Solution ?

Energy Diagram of Li-Ion Battery (Open Circuit State)

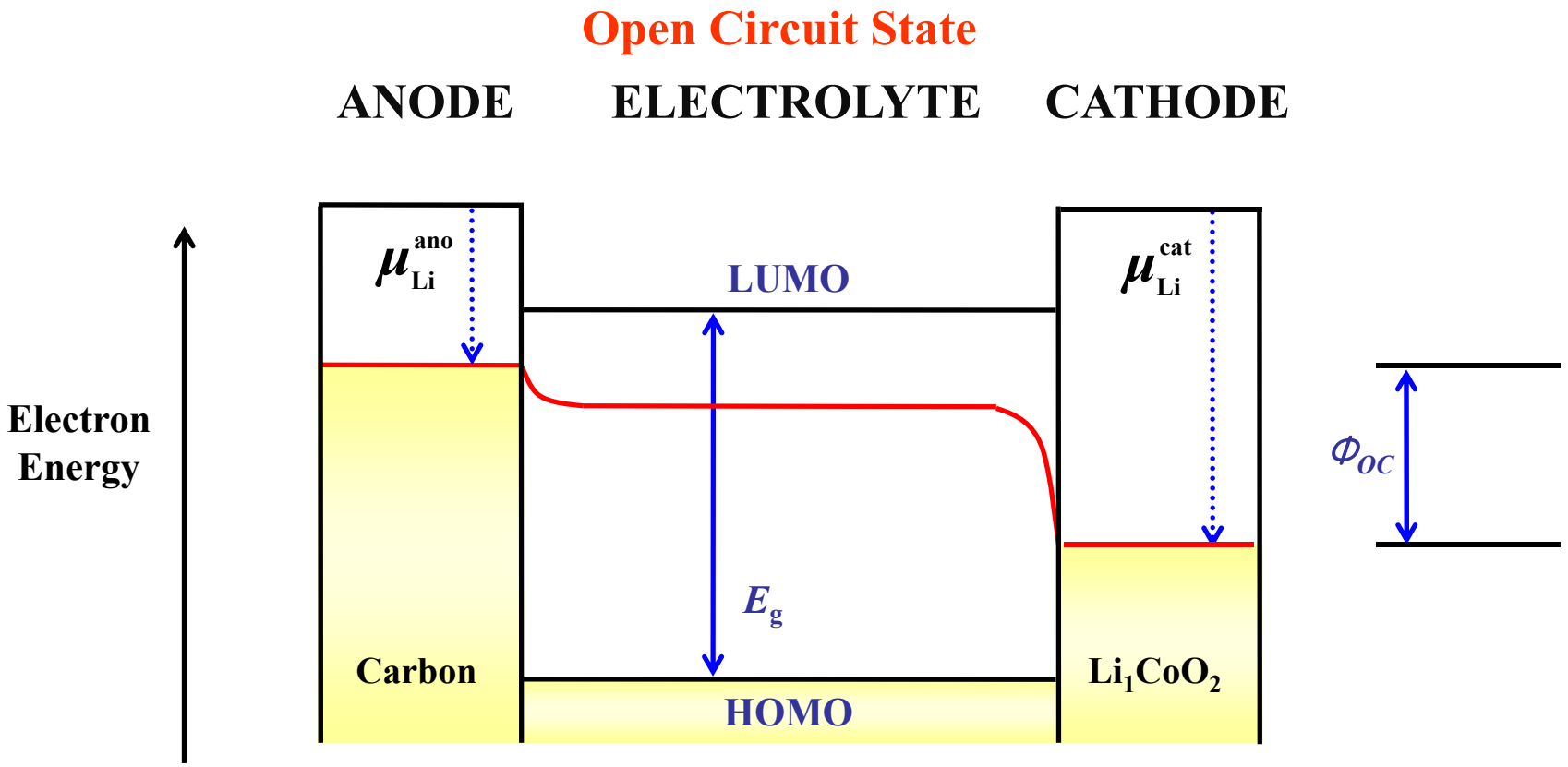

- **LUMO: Lowest Unoccupied Molecular Orbital**
- **HOMO: Highest Occupied Molecular Orbital**

Energy Diagram of Li-Ion Battery (Charge)

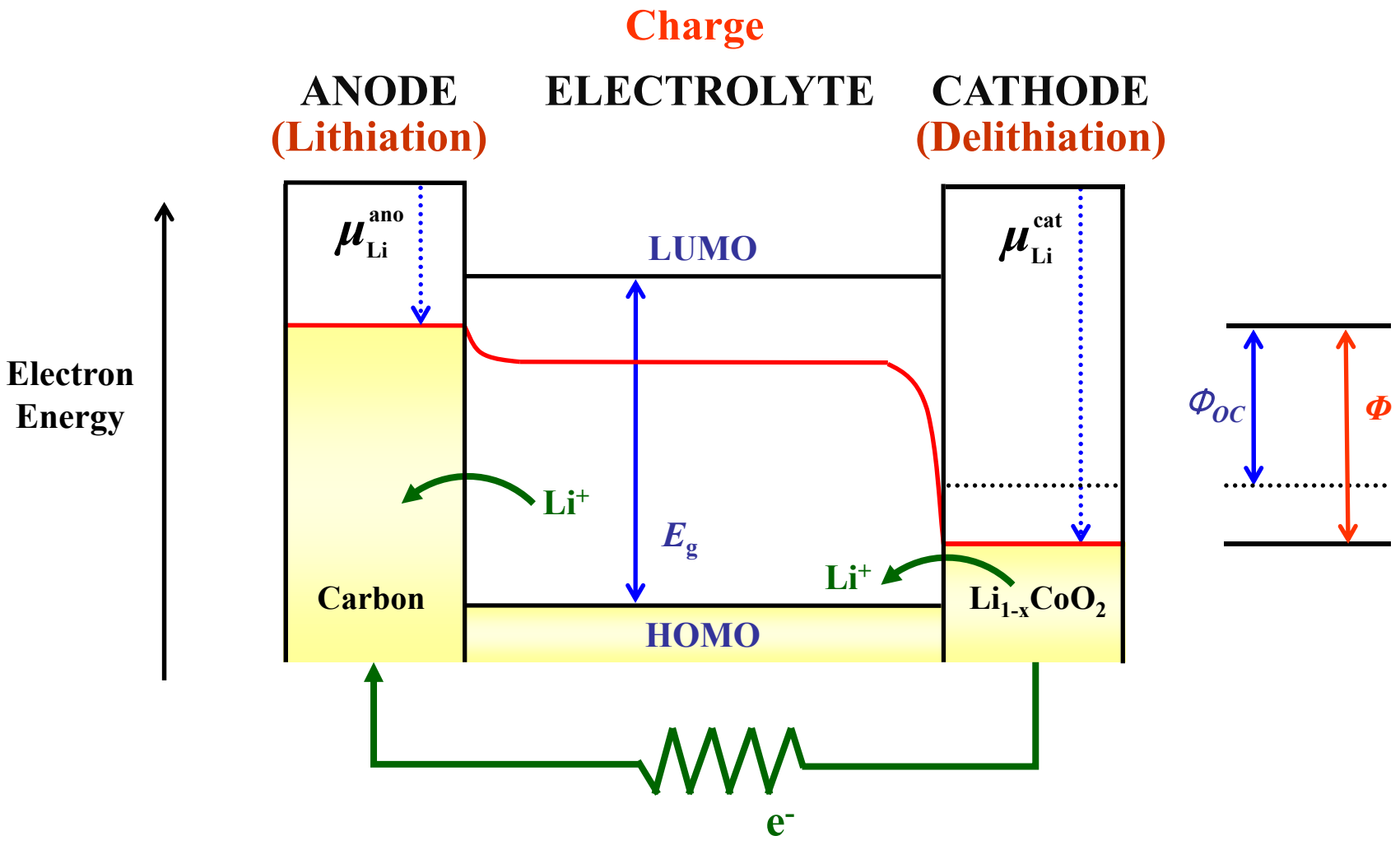

Energy Diagram of Li-Ion Battery (Discharge)

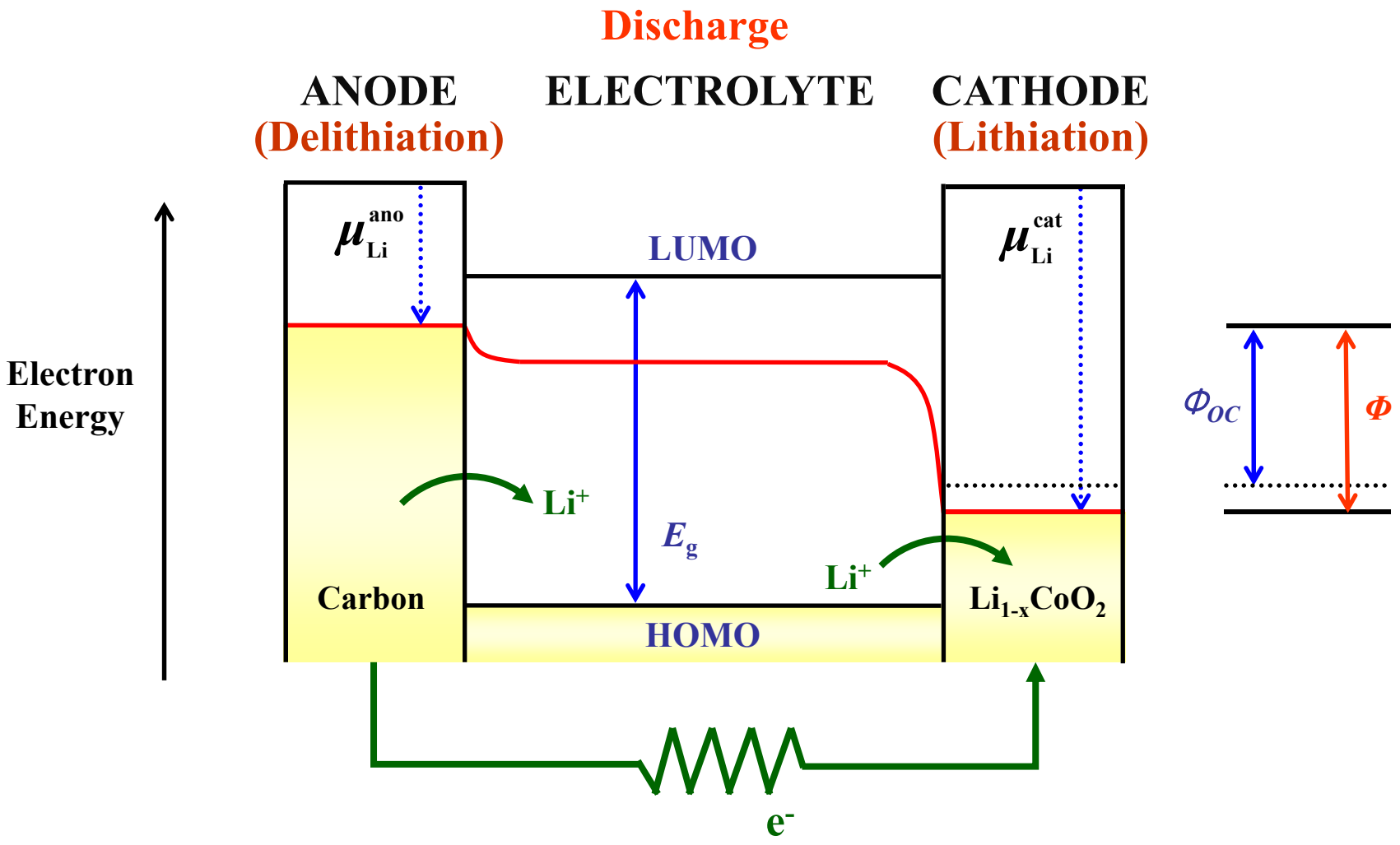

Degradation Mechanisms

1. **With residual H_2O, formation of HF:**

$LiCF_3SO_3 > LiPF_6 > LiClO_4 > LiAsF_6 > LiBF_4$

$LiPF_6 + H_2O \rightarrow LiF + 2HF + POF_3$

$PF_5 + H_2O \rightarrow 2HF + POF_3$

2. Remaining H^+ can react with the spinel $LiMn_2O_4$, forming H_2O.

$2LiMn_2O_4 + 4H^+ \rightarrow 2Li^+ + Mn^{2+} + 2H_2O + 3\lambda\text{-}MnO_2$

Degradation Mechanisms

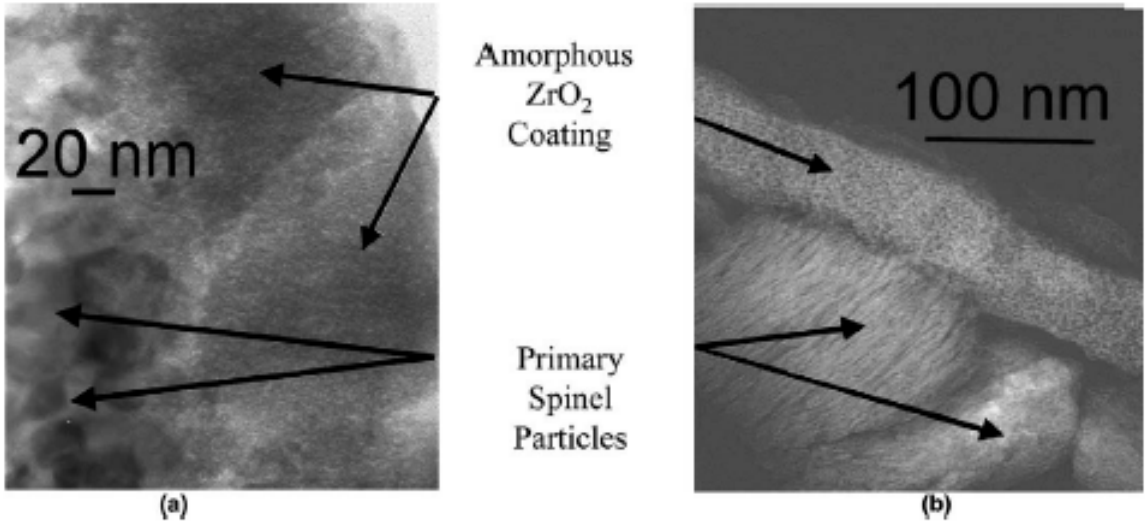

Fig. 1. TEM images of $LiMn_2O_4$ spinel particles with an amorphous ZrO_2 coating.

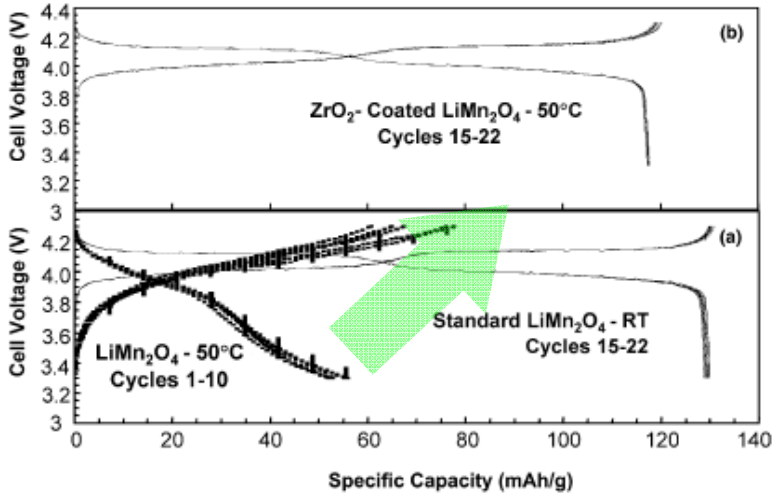

Fig. 2. Comparison of the electrochemical cycling stability of lithium cells with (a) uncoated $LiMn_2O_4$ electrodes at room temperature and 50 °C, and (b) ZrO_2-coated $LiMn_2O_4$ electrodes at 50 °C.

ZrO_2 coated spinel $LiMn_2O_4$ 에서 50°C 충방전시 성능향상 (50°C 에서 H^+와 반응 가속; uncoated $LiMn_2O_4$ 는 열화가 심함)

ZrO_2 coating can scavenge HF attack.

Thackeray *et al.*, *Electrochem. Comm.* **5**, 752 (2003)

Argonne National Laboratory

ZrO_2- and Li_2ZrO_3-Stabilized Spinel and Layered Electrodes

Abstract

Strategies for countering the solubility of $LiMn_2O_4$ (spinel) electrodes at 50 °C and for suppressing the reactivity of layered $LiMO_2$ (M = Co, Ni, Mn, Li) electrodes at high potentials are discussed. Surface treatment of $LiMn_2O_4$ with colloidal zirconia (ZrO_2) dramatically improves the cycling stability of the spinel electrode at 50 °C in $Li/LiMn_2O_4$ cells. ZrO_2-coated $LiMn_{0.5}Ni_{0.5}O_2$ electrodes provide a superior capacity and cycling stability to uncoated electrodes when charged to a high potential (4.6 V vs Li^0). The use of Li_2ZrO_3, which is structurally more compatible with spinel and layered electrodes than ZrO_2 and which can act as a Li^+-ion conductor, has been evaluated in composite $0.03Li_2ZrO_3 \cdot 0.97LiMn_{0.5}Ni_{0.5}O_2$ electrodes; glassy $Li_xZrO_{2+x/2}$ $(0 < x \leqslant 2)$ products can be produced from colloidal ZrO_2 for surface coatings.

Keywords: Lithium batteries; Stabilized electrode; Spinel; Layered; Zirconia; Coating

Thackeray *et al.*
Argonne National Laboratory
Electrochem. Comm. **5**, 752 (2003).

Anode for Li^+ Battery

Anodes and Composite Anodes: An Overview

Table 4.1. Capacities and volume changes of different elements.

Starting material	C	Al	Si	Sn	Bi
Lithiated phase	LiC_6	Li_9Al_4	$Li_{21}Si_5$	$Li_{17}Sn_4$	Li_3Bi
Theoretical specific capacity (Ah/kg)	372	2235	4010	959	385
Theoretical volumetric capacity (Ah/l)	833	6035	9340	7000	3773
Volume changes (%)	12	238	297	257	115

$C \leftrightarrow LiC_6$

Δa axis ~ 1%

Δc axis ~ 10%

ΔV ~ 12%

Lithium Batteries – Science and Technology
edited by G.-A. Nazri and G. Pistoia

N. A. W. Holzwarth's group
(Exxon Research and Engineering Company)
Physical Review B **28**, 1013 (1983).

Short Circuiting due to Li Crystal Growth

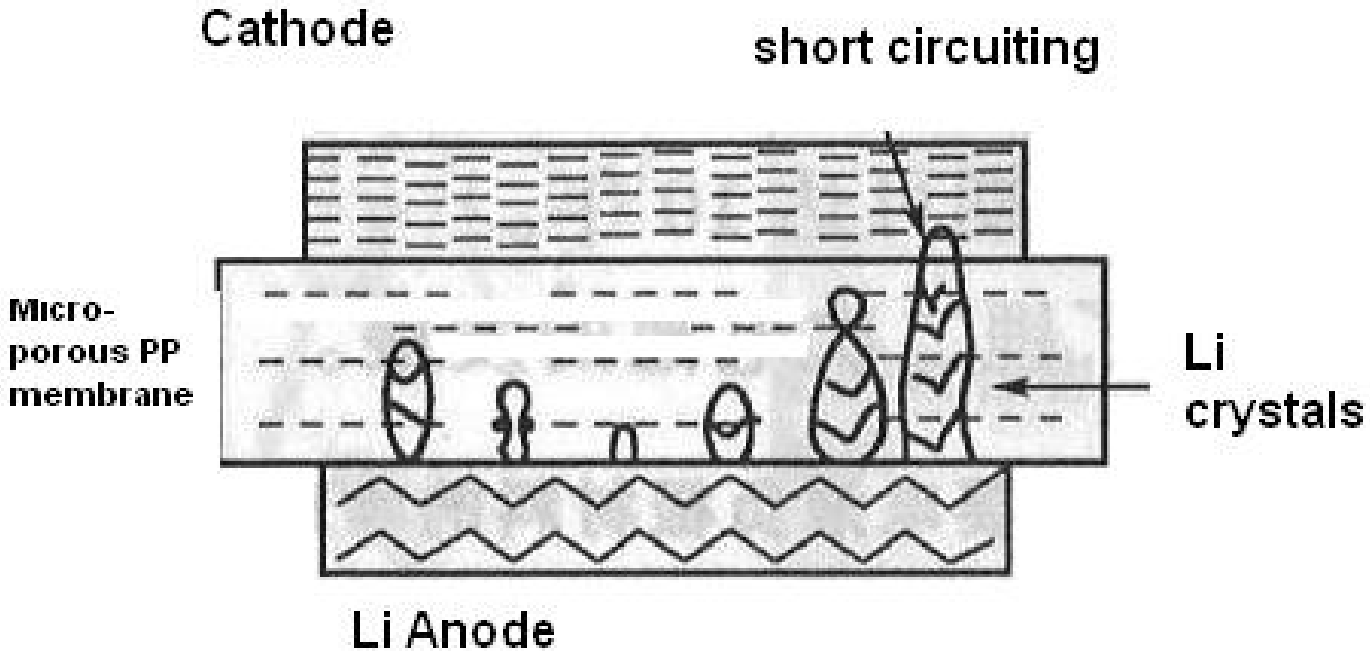

Lithium Batteries – Science and Technology
edited by G.-A. Nazri and G. Pistoia

Lithium-Intercalated Graphite

Lithium-intercalated graphite: Self-consistent electronic structure for stages one, two, and three

N. A. W. Holzwarth*
Corporate Research—Sciences Laboratory, Exxon Research and Engineering Company, P. O. Box 45, Linden, New Jersey 07036

Steven G. Louie
Department of Physics, University of California, Berkeley, California 94720

Sohrab Rabii
Moore School of Electrical Engineering, University of Pennsylvania, Philadelphia, Pennsylvania 19104
(Received 23 February 1983)

First-principles electronic structure calculations were carried out for LiC_6, LiC_{12}, and LiC_{18} representing first-, second-, and third-stage model graphite intercalation compounds. By comparing the charge density of these compounds to that of reference graphite compounds, we could define a "total difference density" in order to quantify charge transfer and polarization in these materials. The total difference density is found to be highly concentrated near the intercalant ions. However, the conduction electrons (those in partially occupied bands) are found to have the distribution of virtually undistorted π wave functions and have a much more delocalized distribution than that of the total difference density. These two types of charge distributions account for many of the unusual electronic properties of graphite intercalation compounds.

N. A. W. Holzwarth's group
(Exxon Research and Engineering Company)
Physical Review B **28**, 1013 (1983).

Remaining Challenges in Thin-Film Battery

Electrode: Novel Electrode with High Thermal/Electrochemical Stability
Electrolyte: Nanostructure-Controlled Solid Electrolyte

Current Collector: Metal or Metal Compounds
Substrate: Various Substrates such as Si Wafer, Flexible Polymer, etc.

Designs: Pile-Up Process for Capacity Control

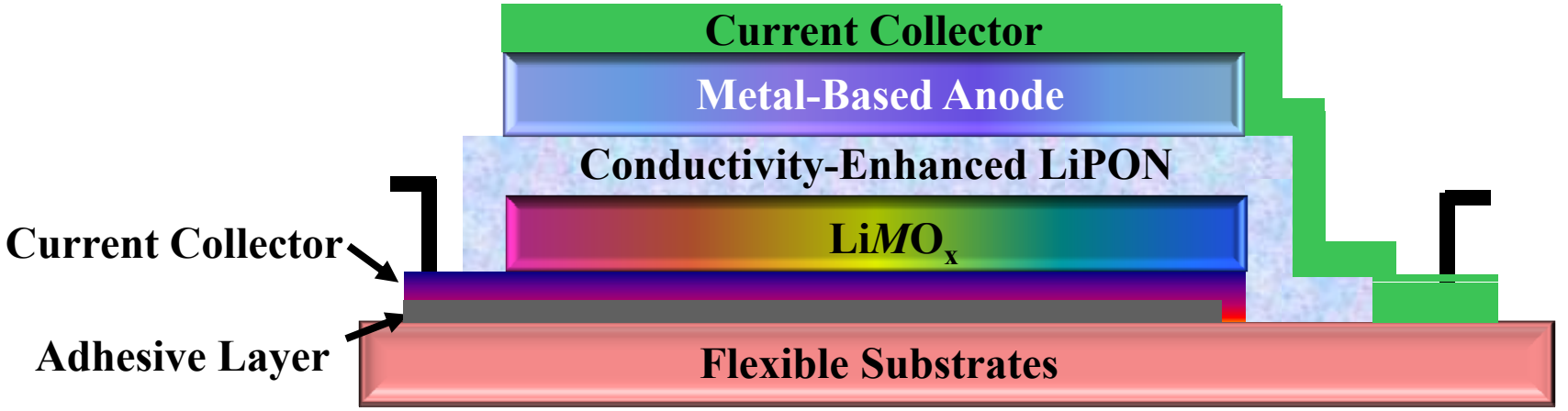

Advances Toward Next-Generation Flexible Battery

Technological improvements in rechargeable solid-state batteries are being driven by an ever-increasing demand for portable electronic devices. Lithium-ion batteries are the systems of choice, offering high energy density, flexible and lightweight design, and longer lifespan than comparable battery technologies. We present a brief historical review of the development of lithium-based rechargeable batteries, highlight ongoing research strategies, and discuss the challenges that remain regarding the synthesis, characterization, electrochemical performance and safety of these systems

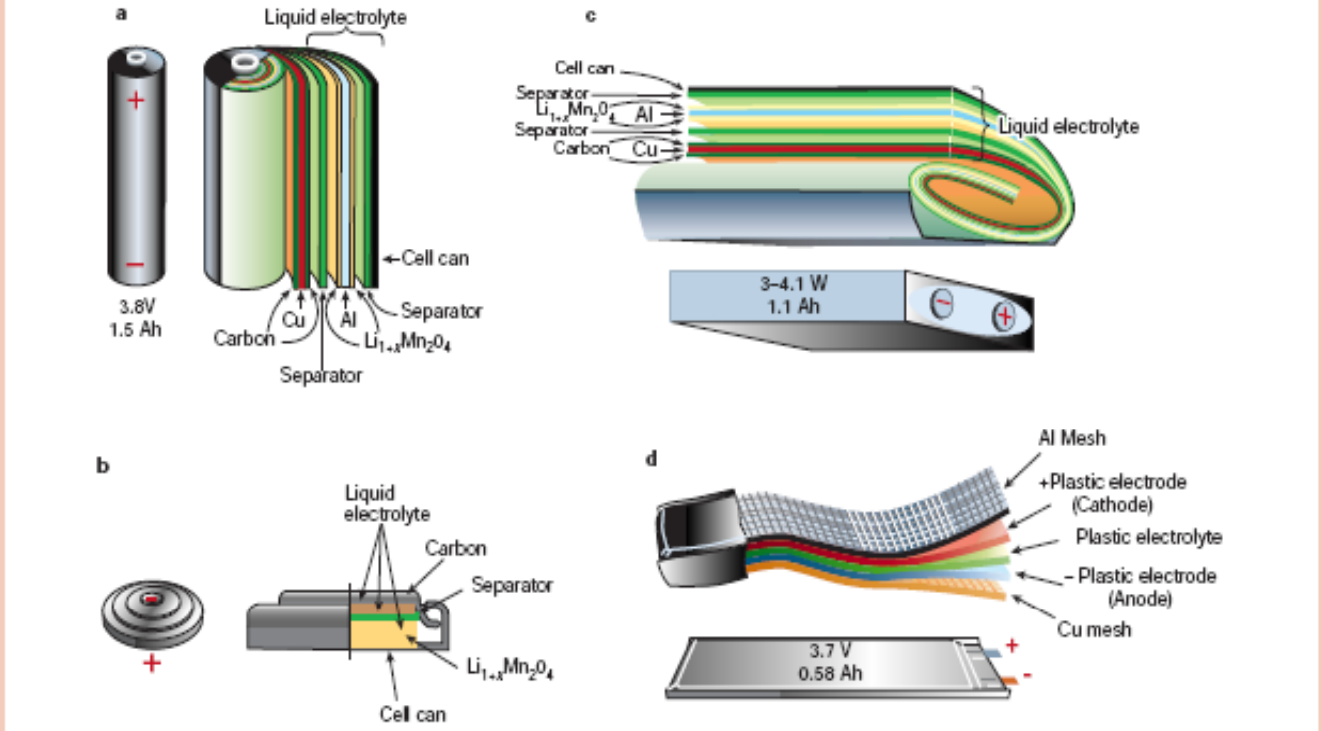

Figure 4 Schematic drawing showing the shape and components of various Li-ion battery configurations. a, Cylindrical; b, coin; c, prismatic; and d, thin and flat. Note the unique flexibility of the thin and flat plastic LiION configuration; in contrast to the other configurations, the PLiION technology does not contain free electrolyte.

Plastic Li-Ion Battery

J.-M. Tarascon *et al.*
Nature (2001)

Advances Toward Next-Generation Flexible Battery

Batteries power a wide range of electronic devices including phones, laptop computers and medical devices such as cardiac pacemakers and defibrillators. In the near future, batteries may also help fight global warming by improving the performance of electric or hybrid vehicles with zero or reduced carbon emissions. With the ever-increasing demand for efficiency and design, there is a need for ultrathin, safe and flexible energy storage options.

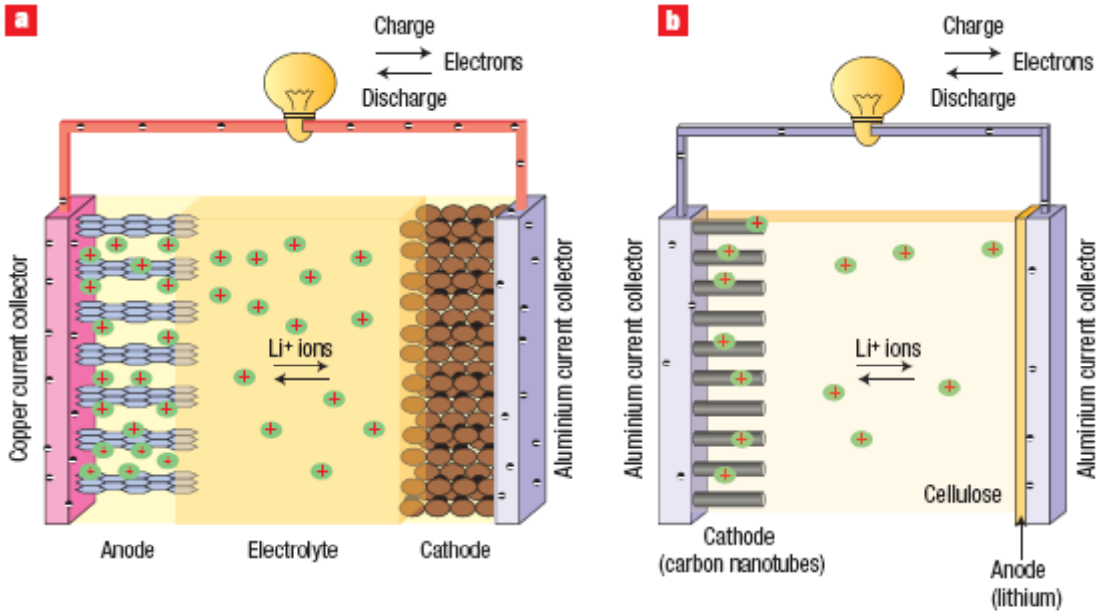

Figure 1 Schematic of different battery configurations. **a**, A conventional lithium-ion battery contains a graphite anode (grey hexagons), a lithium cathode (lithium cobalt oxide in this case; brown circles), and a liquid electrolyte containing lithium ions (green) in a fibre separator (orange). The removal of lithium ions by the simultaneous oxidation of cobalt in the cathode and insertion of lithium ions into the graphite anode charges the battery. Electricity is produced when ions move in the opposite direction and the cobalt is reduced. **b**, A lithium-ion battery made from nanocomposite paper is more compact and weighs less than a conventional lithium-ion battery. The paper, which is made by infiltrating cellulose into carbon nanotubes grown on a silicon substrate, is impregnated with the electrolyte, thus combining the cathode (the nanotubes) and the separator (the cellulose) in a single unit. Depositing a thin film of lithium on one side of the paper and adding aluminium current collectors completes the battery configuration. Electricity is produced when lithium is oxidized to form lithium ions, which are inserted into the nanotube cathode. Charging occurs when the ions move in the opposite direction and are deposited as lithium metal.

CNT and Cellulose-Based Paper-Type Battery

Bruce Scrosati

Nature Nanotechnology (2007)

Advances Toward Next-Generation Flexible Battery

The design of soft portable electronic equipment, such as rollup displays and wearable devices, requires the development of batteries that are flexible. Active radio-frequency identification tags and integrated circuit smart cards also require bendable or flexible batteries for durability in daily use. Several routes toward the development of flexible batteries are being explored. Some involve batteries made mostly or entirely from plastic, with the added advantage of avoiding ignitable and toxic substances such as lithium and lead. An inorganic primary battery that can be bent like a piece of paper has been developed for disposable-card applications (*1*, *2*). However, primary batteries produce current by a one-way chemical reaction and are not rechargable; their usefulness of in portable electronic equipment is therefore limited. Rechargeable secondary batteries are generally used to power portable equipment. There have been recent efforts to make secondary lithium-ion batteries into thin films while maintaining their high energy capacity (*3*).

Making a bendable lithium-ion battery requires the development of soft electrode-active materials, such as metal oxide nanoparticles or nanocoatings for cathodes and lithium foil or nanocarbon materials for anodes (*4*, *5*). Virus-templated Co_3O_4 nanowires have been shown to improve the capacity of thin, bendable lithium-ion batteries (*6*). The charging/discharging process of batteries is generally dominated by the electron and counterion transport at the surface of the electrodes. By using nanostruc-

The authors are in the Department of Applied Chemistry, Waseda University, Tokyo 169-8555, Japan. E-mail: nishide@waseda.jp

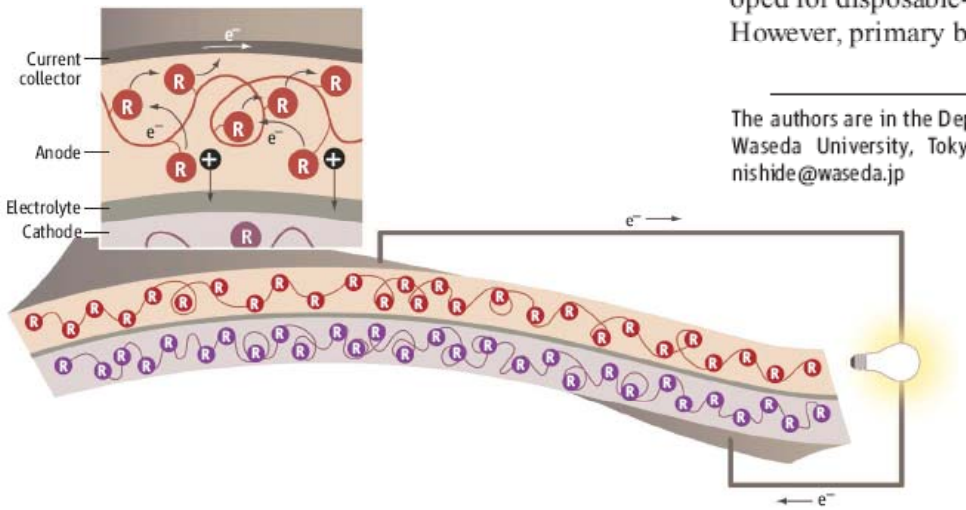

Example of a flexible plastic battery. The R groups in the cathode and in the anode have different redox potentials. During the charging process, charge is stored by oxidizing R groups at the cathode and reducing R groups at the anode. The output voltage of the battery corresponds to the gap between the redox potentials. The curves connecting the R groups are polymer chains, which give flexibility. Many R groups are attached to the polymer chain, so that electrons can hop between neighboring R groups to produce the output current.

Flexible Plastic Battery
Using Organic Polymers

H. Nishide's group
Science (2008)

Advances Toward Next-Generation Flexible Battery

2-Dimensional Assembly of Metal Oxide Nanowires

A. M. Belcher's group
Science (2006)

Virus-Enabled Synthesis and Assembly of Nanowires for Lithium Ion Battery Electrodes

Ki Tae Nam,[1,4] Dong-Wan Kim,[1*] Pil J. Yoo,[2,4] Chung-Yi Chiang,[1,5] Nonglak Meethong,[1] Paula T. Hammond,[2,4] Yet-Ming Chiang,[1] Angela M. Belcher[1,3,4,5]†

The selection and assembly of materials are central issues in the development of smaller, more flexible batteries. Cobalt oxide has shown excellent electrochemical cycling properties and is thus under consideration as an electrode for advanced lithium batteries. We used viruses to synthesize and assemble nanowires of cobalt oxide at room temperature. By incorporating gold-binding peptides into the filament coat, we formed hybrid gold–cobalt oxide wires that improved battery capacity. Combining virus-templated synthesis at the peptide level and methods for controlling two-dimensional assembly of viruses on polyelectrolyte multilayers provides a systematic platform for integrating these nanomaterials to form thin, flexible lithium ion batteries.

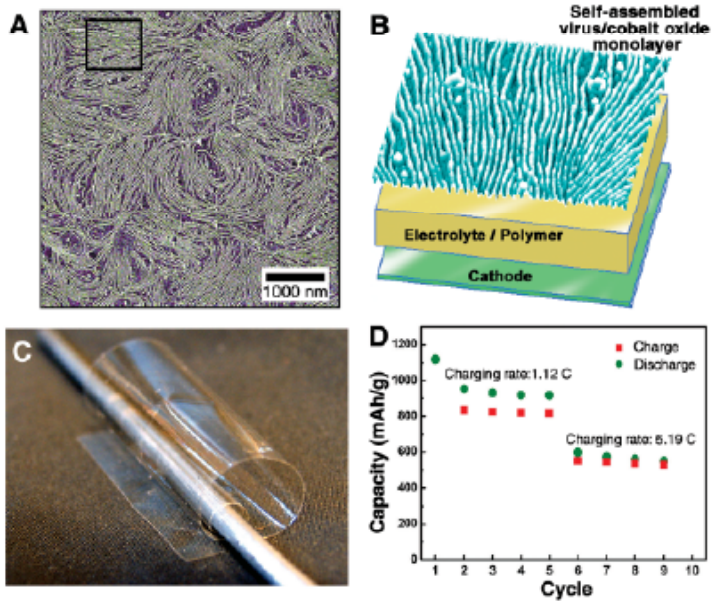

Fig. 4. Two-dimensional assembly of Co_3O_4 nanowires driven by liquid crystalline ordering of the engineered M13 bacteriophage viruses. (**A** and **B**) Phase-mode atomic force microscope image of macroscopically ordered monolayer of Co_3O_4-coated viruses. The Z range is 30° (**C**) Digital camera image of a flexible and transparent free-standing film of $(LPEI/PAA)_{100.5}$ on which Co_3O_4 viral nanowires are assembled into nanostructured monolayer with dimensions of 10 cm by 4 cm. (**D**) Capacity for the assembled monolayer of Co_3O_4 nanowires/Li cell at two different charging rates.

The Effect of Metal-Oxide Coating in $LiCoO_2$ Cathodes

Structure of $LiCoO_2$

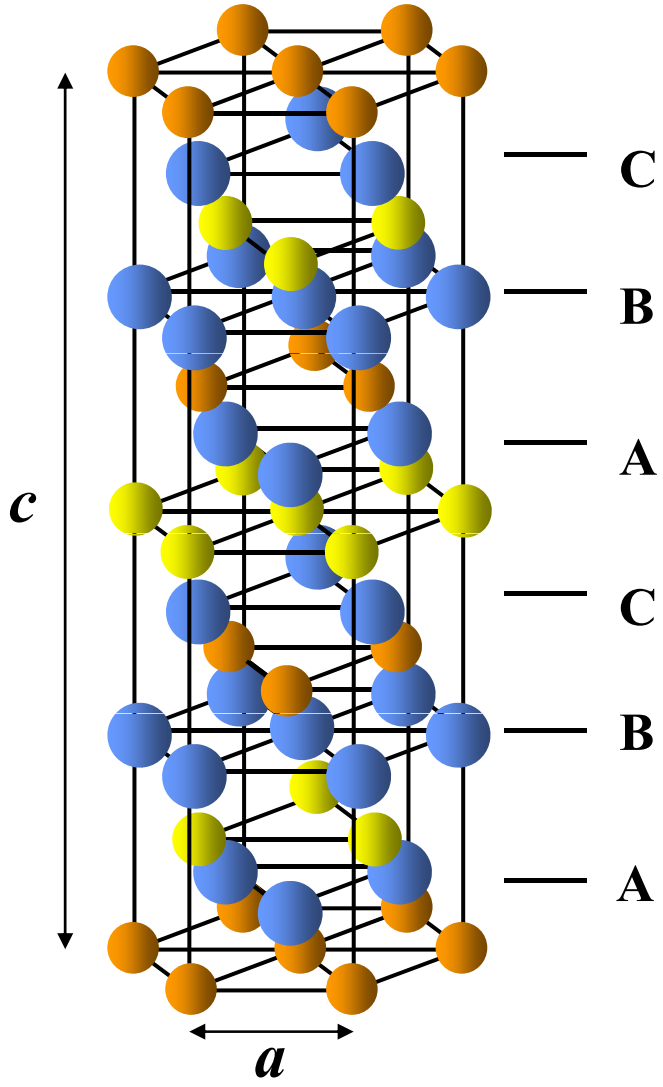

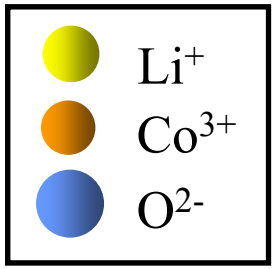

$Li_{1-x}CoO_2$ for $0 < x < 0.5$

Space group: $R\bar{3}m$
a = 2.81 Å and c = 14.08 Å

Structure of $LiCoO_2$

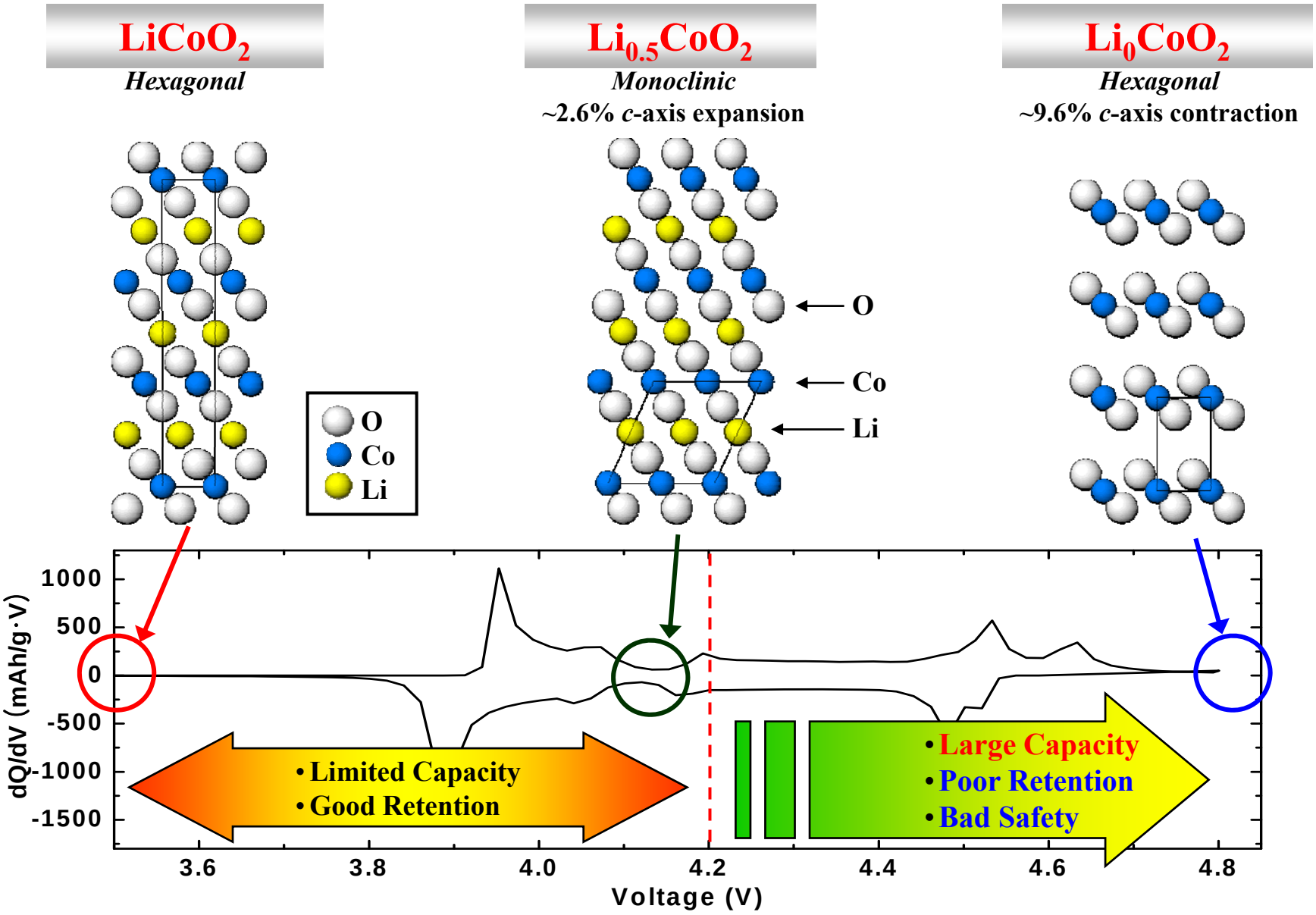

Mechanisms of Capacity Fading and Safety

❖ Cobalt Loss from $Li_{1-x}CoO_2$

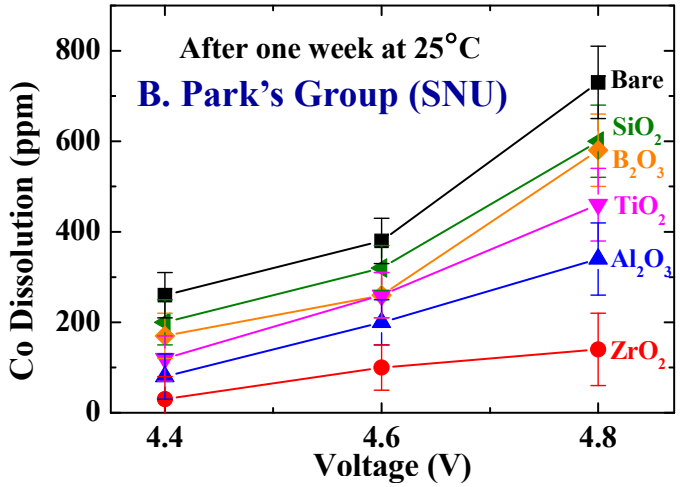

❖ Structural Instability

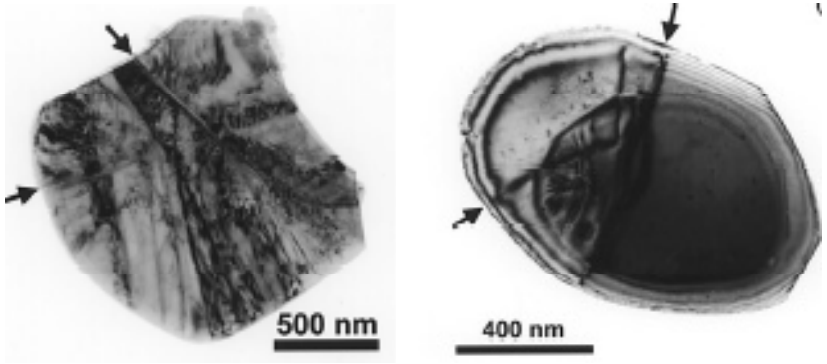

Y.-M. Chiang's Group (MIT)

❖ Oxygen Loss from $Li_{1-x}CoO_{2-\delta}$

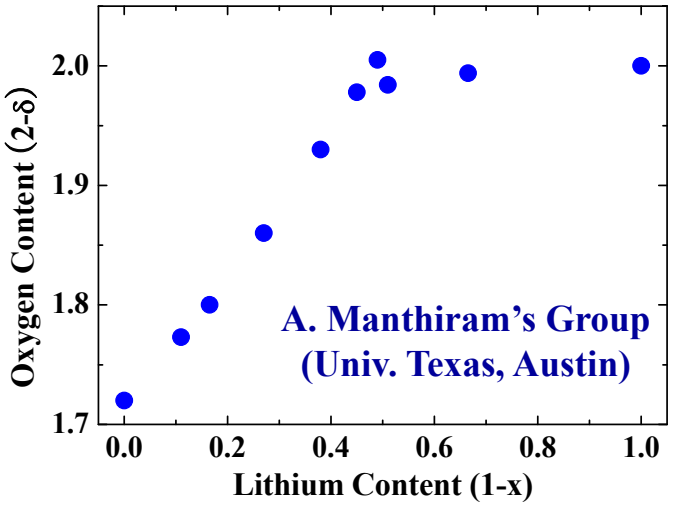

❖ Exothermic Reaction with Electrolyte

http://www.citynews.ca

Capacity Retention of Metal-Oxide-Coated $LiCoO_2$

❖ **Li/Metal-Oxide-Coated $LiCoO_2$**

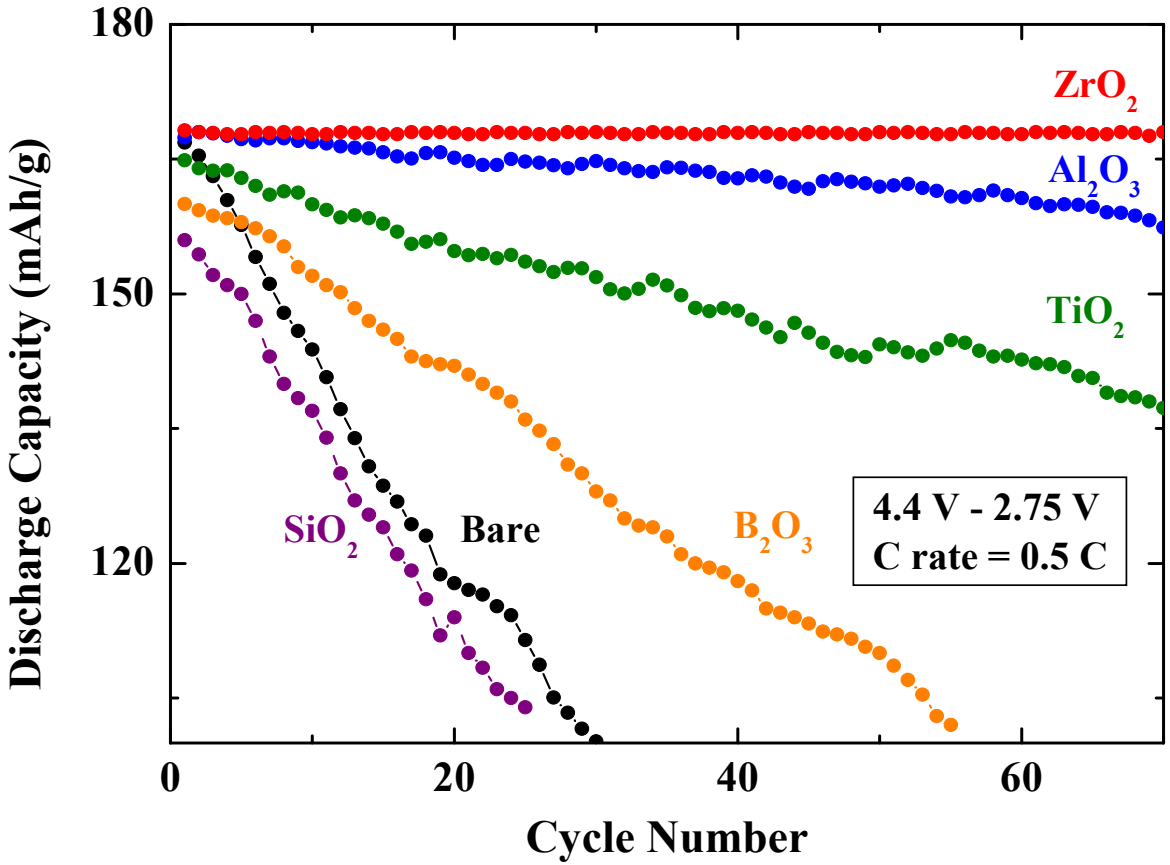

Moderate Metal-Oxide Coating on Cathode

Enhanced Capacity Retention by Protection of Surface

➢ J. Cho, Y. J. Kim, T.-J. Kim, and B. Park *Angew. Chem. Int. Ed.* **40**, 3367 (2001).

Charge-Discharge Experiments in Thin Films

Uncoated $LiCoO_2$ Thin Film

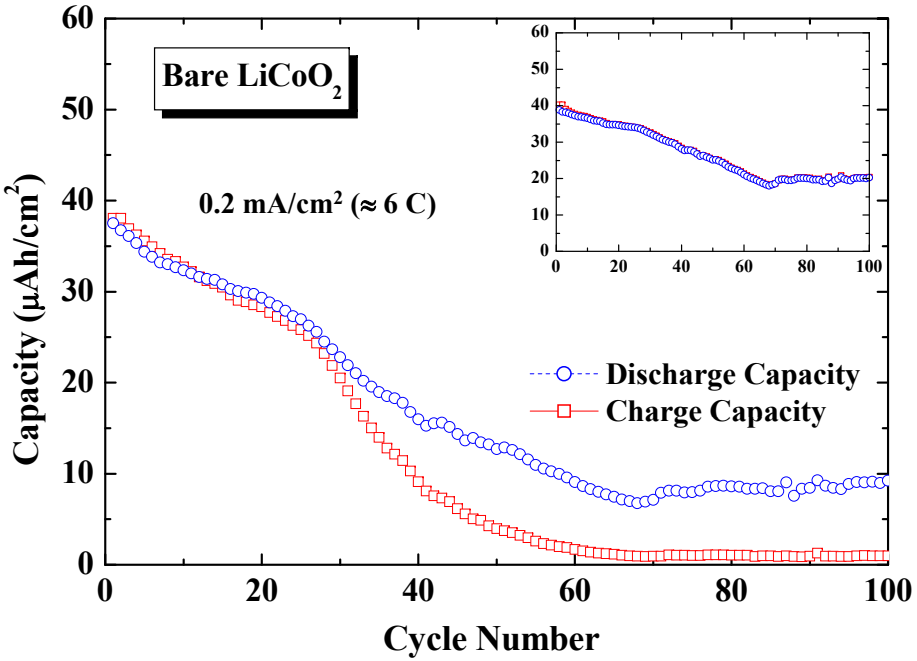

Al_2O_3-Coated $LiCoO_2$ Thin Film

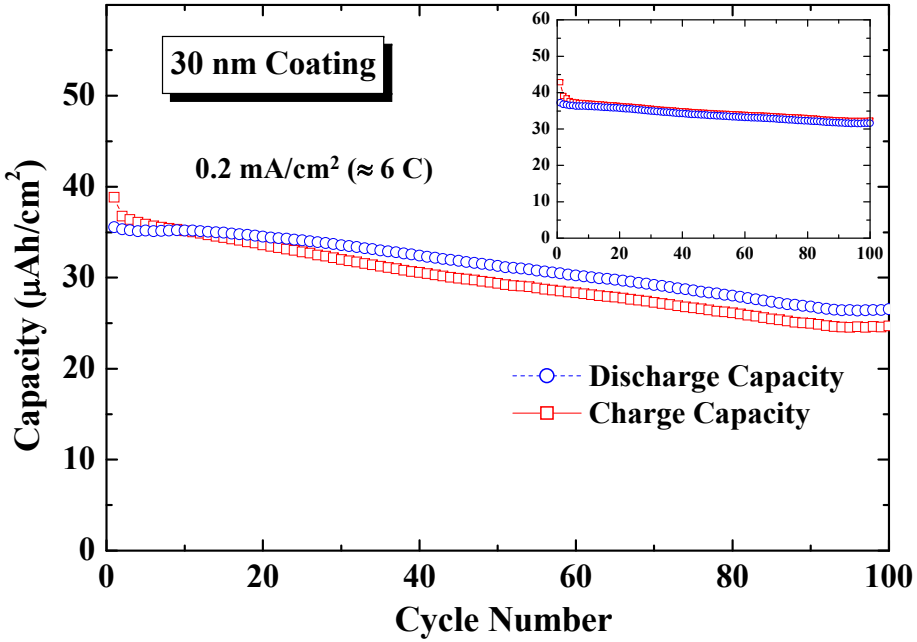

The charge capacity (for Li deintercalation) shows faster deterioration than the discharge capacity (for Li intercalation).

- Cell voltage : 4.4 V - 2.75 V
- Current rates : 0.1 - 0.8 mA/cm²
- Half-cells (Li/$LiCoO_2$), 1 M $LiPF_6$ in EC/DEC
- At each cutoff step, the voltage was potentiostated until the current decreased to 10%.

Al_2O_3 Coating Layer as a Solid Electrolyte

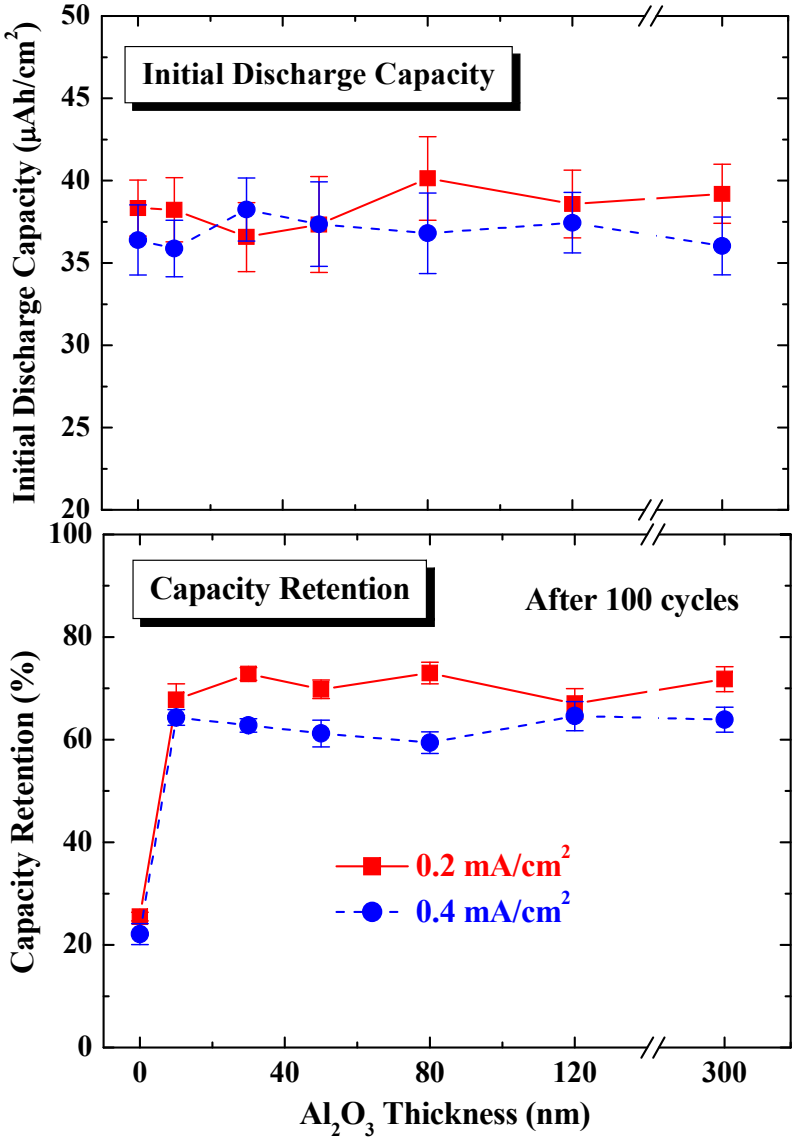

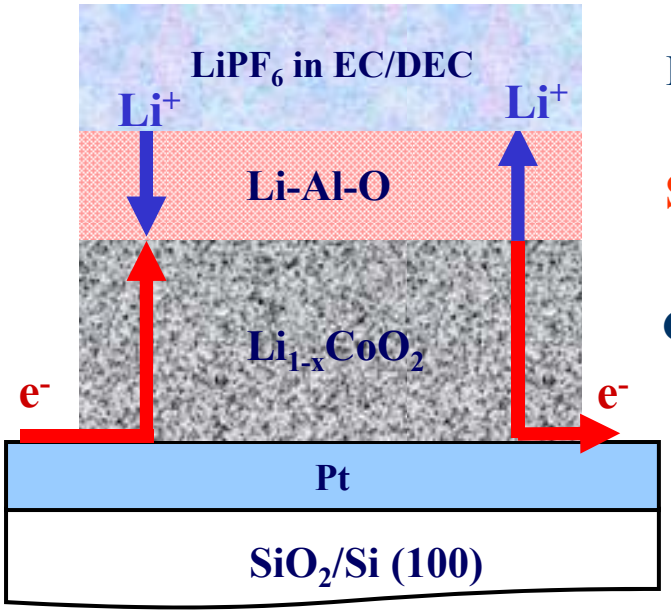

Liquid Electrolyte

Solid Electrolyte

Cathode

Current Collector

Substrate

Oxidation/reduction reaction occurs at the Li-Al-O / $LiCoO_2$ interface.

Composition of Li-Al-O needs to be determined.

Ex) $0.7Li_2O$-$0.3Al_2O_3$: ~10^{-7} S/cm at 23°C

A. M. Glass *et al.*, *J. Appl. Phys.* (1980).

Apparent Li^+ Diffusivity during Li Deintercalation (Charging)

Uncoated $LiCoO_2$ Thin Film

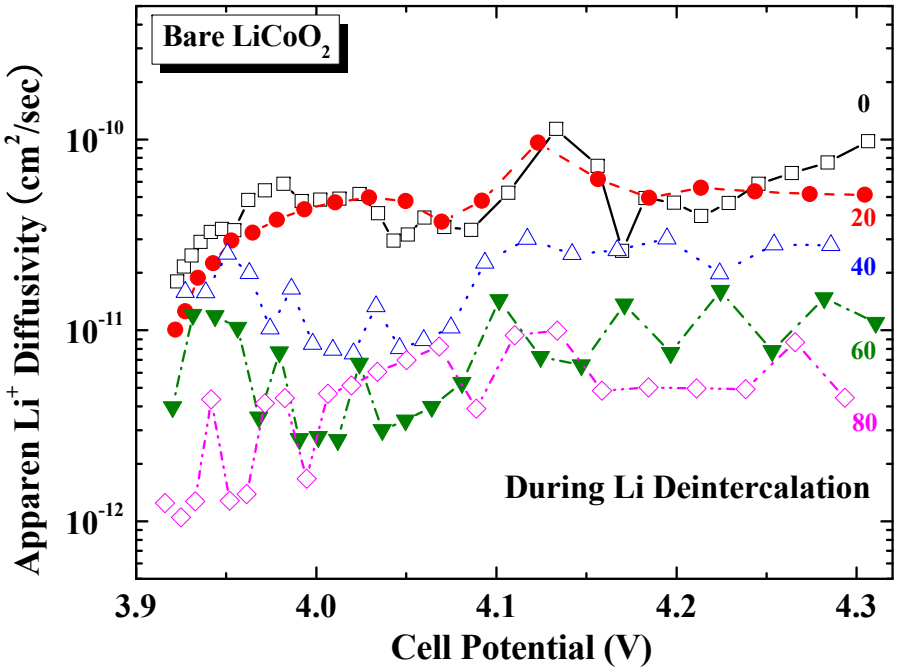

Al_2O_3-Coated $LiCoO_2$ Thin Film

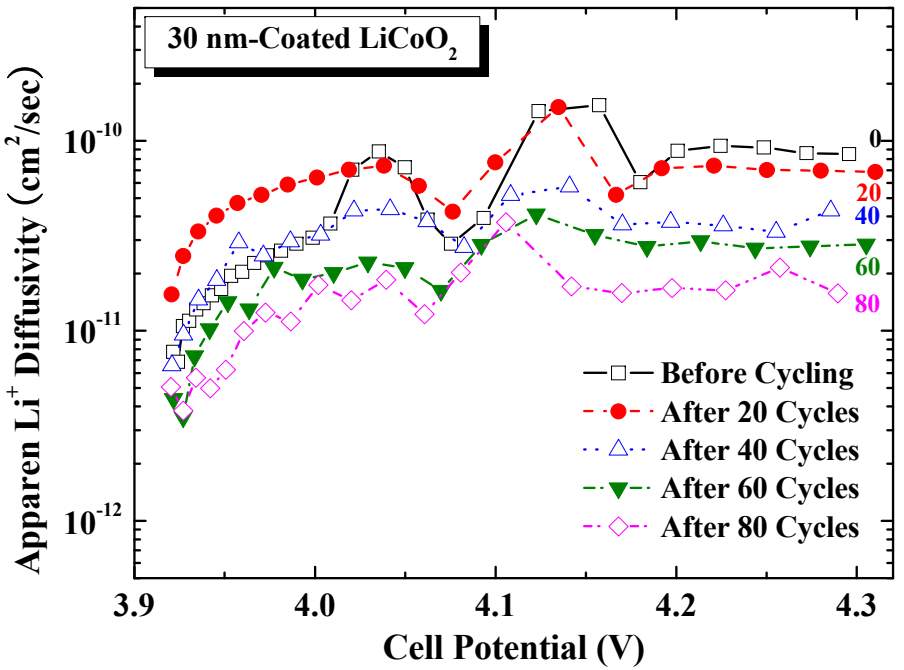

- Clearly enhanced by 30 nm-thick Al_2O_3 coating.
- Maxima at ~4.13 V, corresponding to the monoclinic phase.
- Two minima at the cell potential, corresponding to the phase transition between a hexagonal and monoclinic phase.

The Effect of Metal-Oxide Coating in $LiCoO_2$

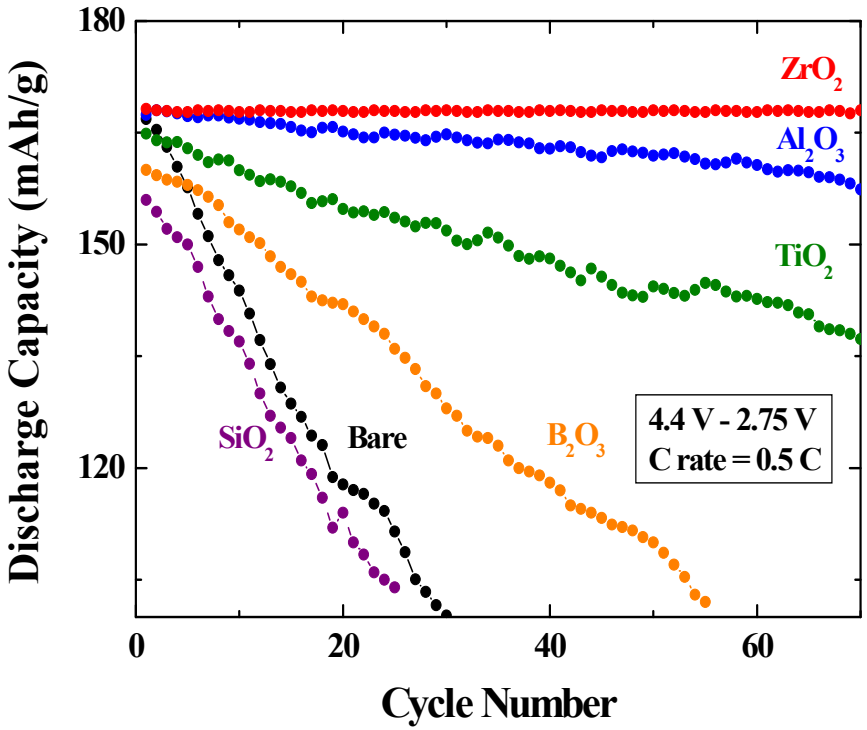

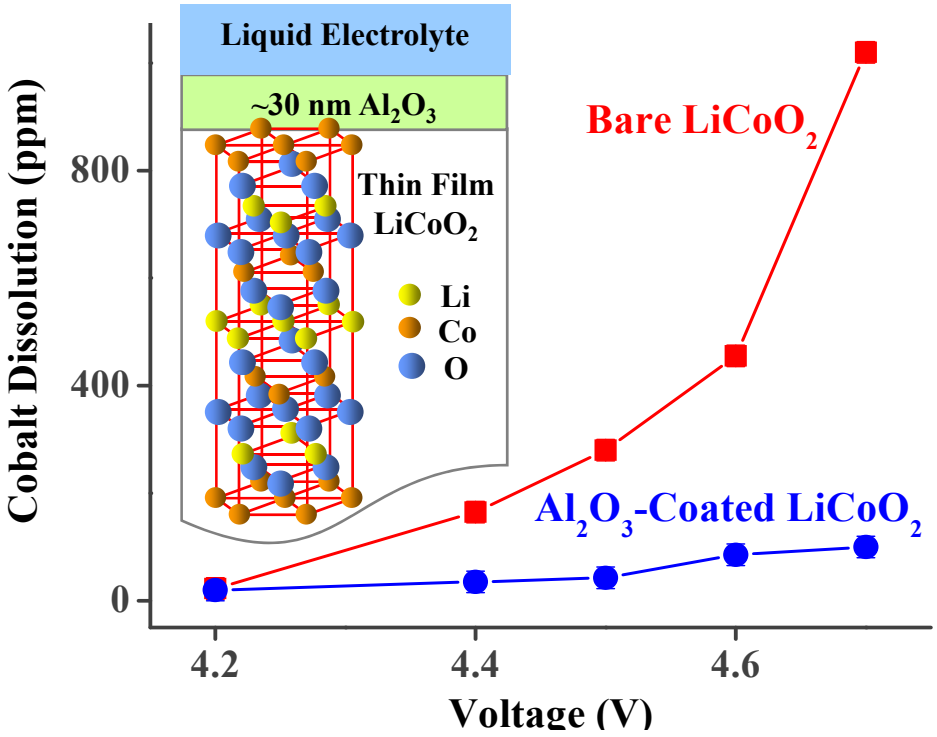

Enhanced Stability by Nanoscale Coating

- J. Cho, Y. J. Kim, T.-J. Kim, and B. Park, *Angew. Chem. Int. Ed.* **40**, 3367 (2001).
- J. Cho, Y. J. Kim, and B. Park, *Chem. Mater.* **12**, 3788 (2000).

HF Scavenging Effect

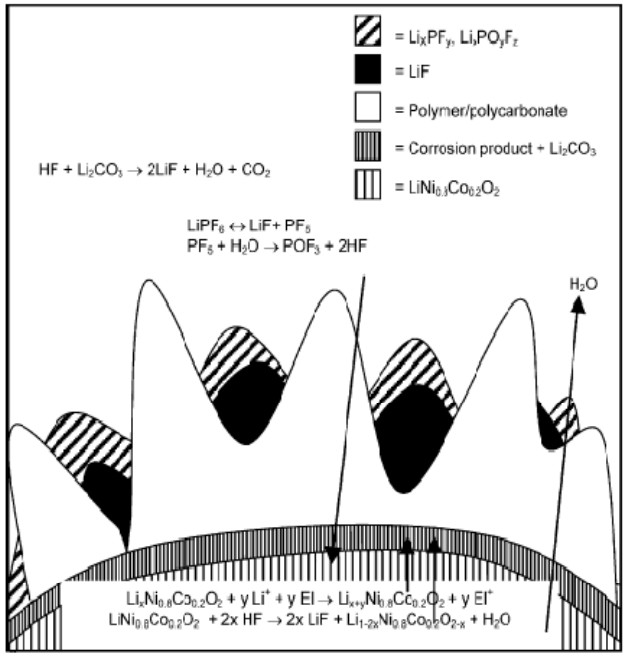

Aurbach's group, *J. Electrochem. Soc.* (1989).
Edstrom's group, *Electrochim. Acta* (2004).

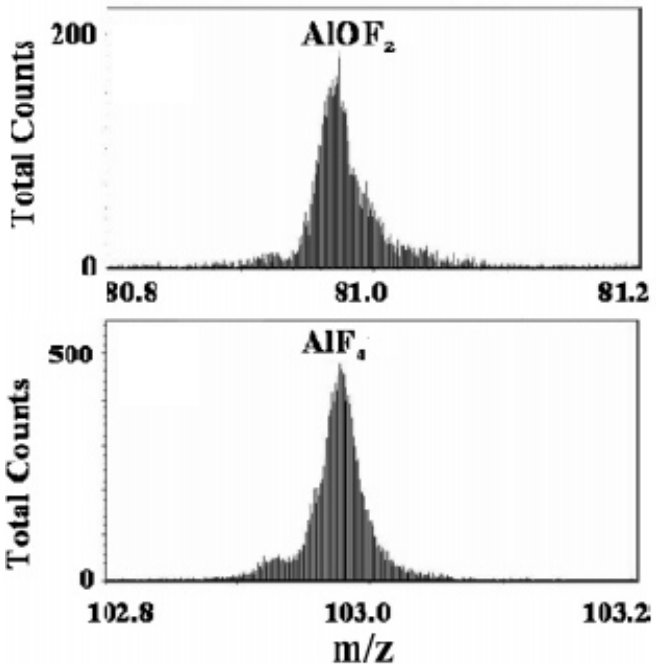

Y.-K. Sun's group, *Chem. Mater.* (2005).

$$LiPF_6 \rightarrow LiF + PF_5$$

$$PF_5 + H_2O \rightarrow 2HF + POF_3$$

$$Al_2O_3 + 6HF \rightarrow 2AlF_3 + 3H_2O$$

Secondary Ion Mass Spectroscopy (SIMS)

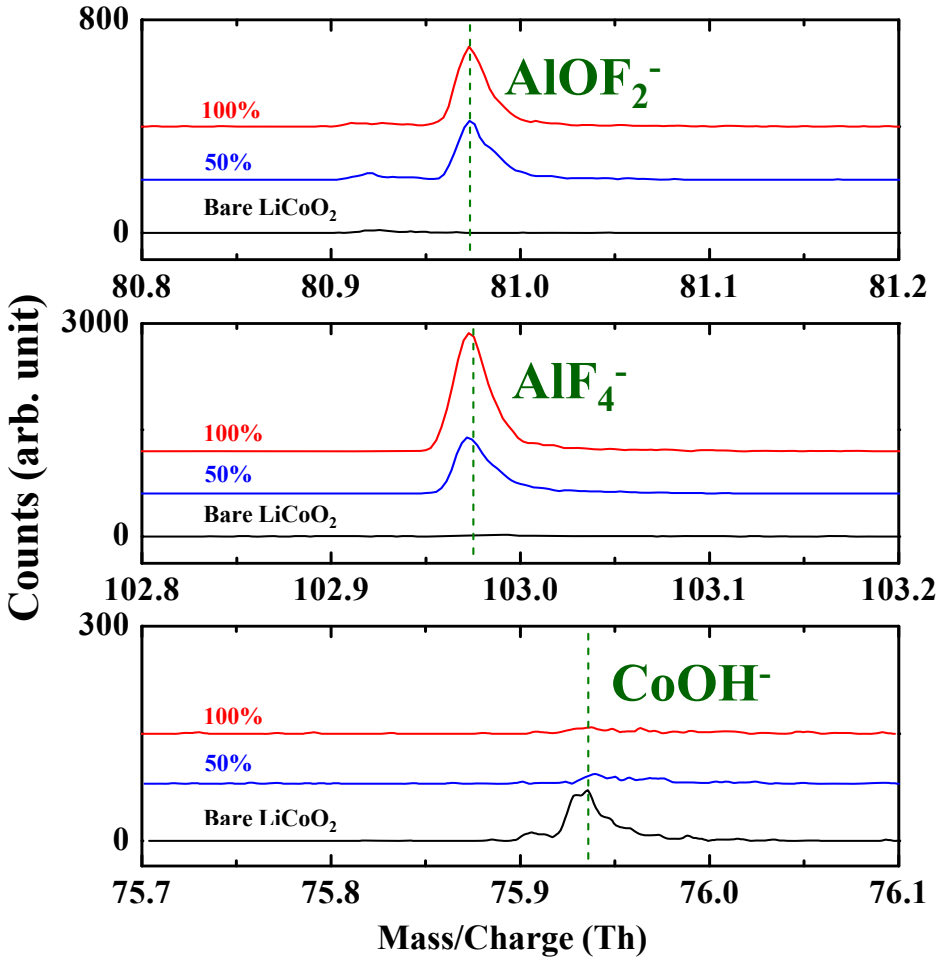

Mass/Charge (Th)
- AlF_4^-: 102.98 Th
- $AlOF_2^-$: 80.97 Th
- $CoOH^-$: 75.94 Th

AlF_4^- and $AlOF_2^-$ from $AlF_3 \cdot 3H_2O$ generated by the reaction among Al_2O_3, HF and H_2O.

Schematic Figure

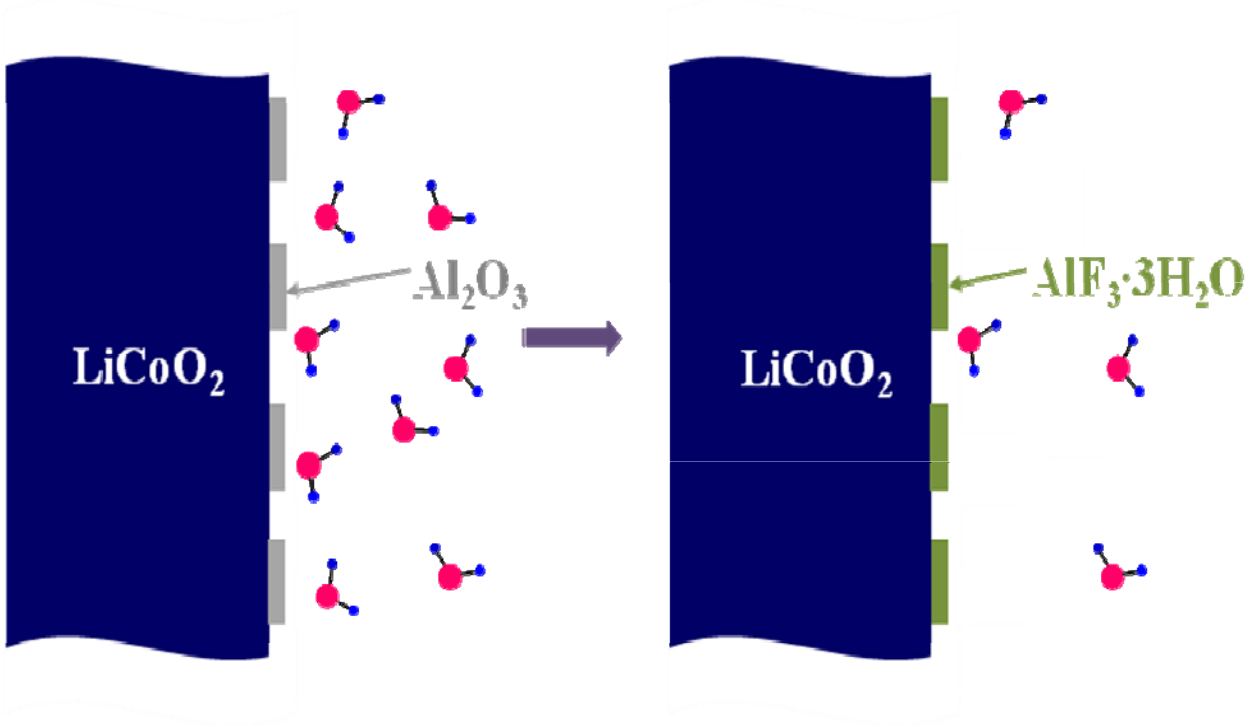

- **Al_2O_3 coating layer: Transformed into $AlF_3 \cdot 3H_2O$ layer**
- **H_2O decreased in the electrolyte.**

Metal-Phosphate-Coated $LiCoO_2$ Cathode Materials

12 V Overcharge Test at 1 C Rate

Bare $LiCoO_2$

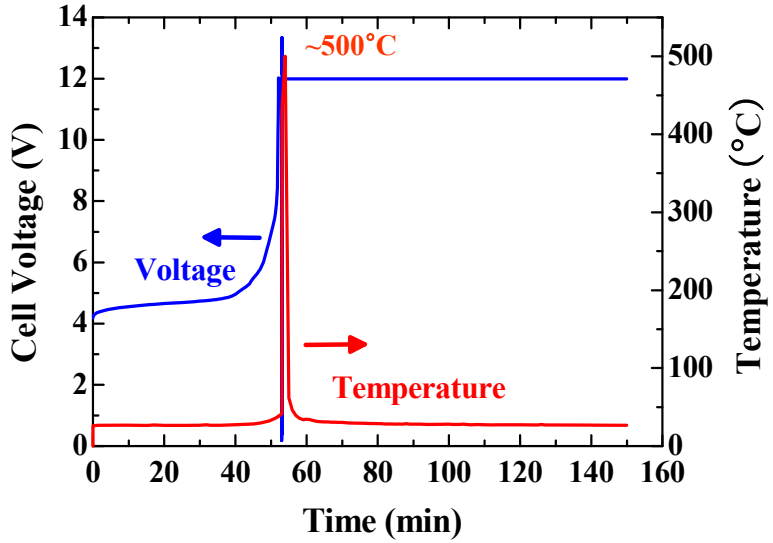

Short Circuit & Temperature Uprise

Cell Fired and Exploded

$AlPO_4$-Coated $LiCoO_2$

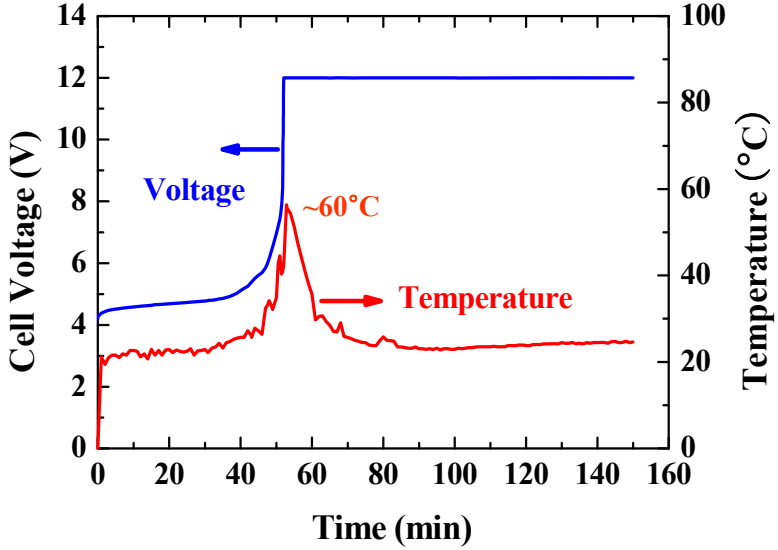

Temperature only ~60°C

Excellent Thermal Stability

➢ B. Park's group, *Angew. Chem. Int. Ed.* (2001).

TEM Image of $AlPO_4$ Nanoparticle-Coated $LiCoO_2$

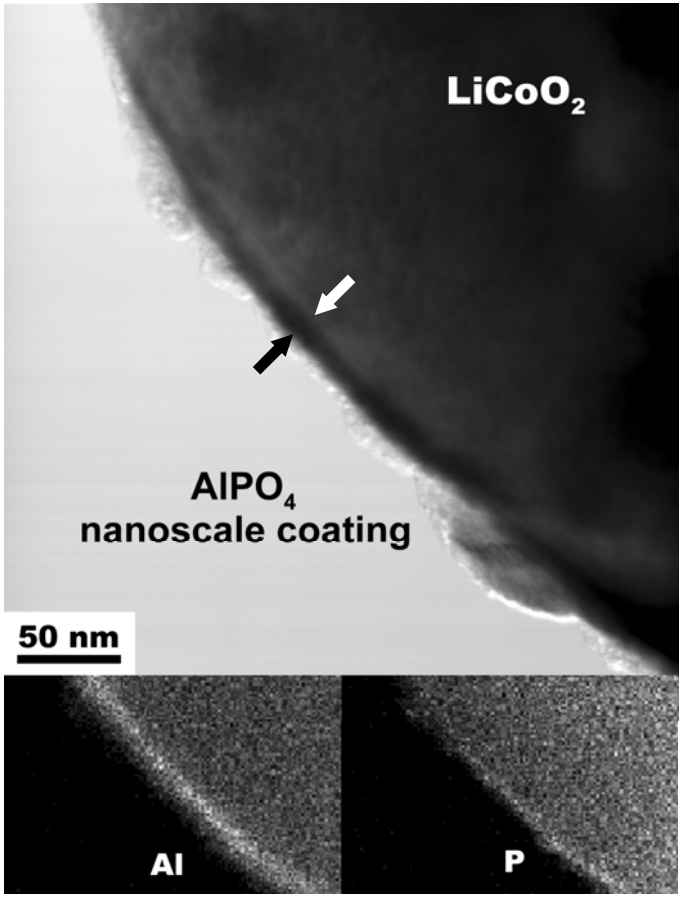

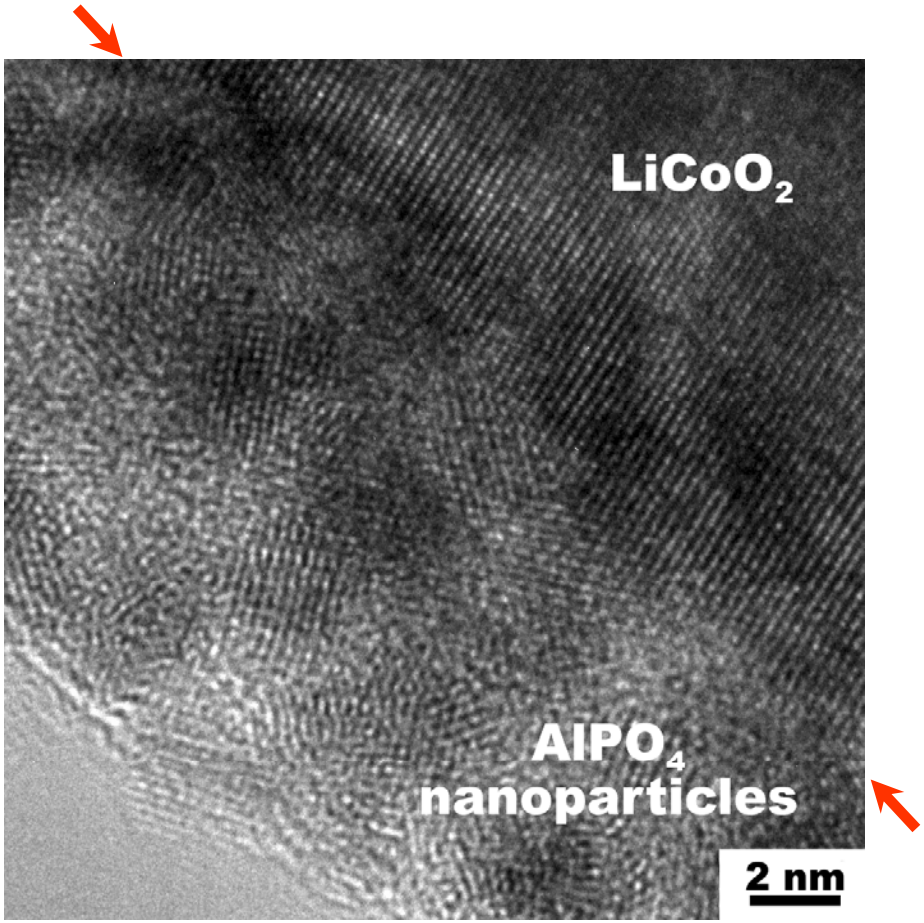

EDS confirms the Al and P components in the nanoscale-coating layer.

$AlPO_4$ nanoparticles (~3 nm) embedded in the coating layer (~15 nm).

$AlPO_4$-Nanoparticle-Coated $LiCoO_2$

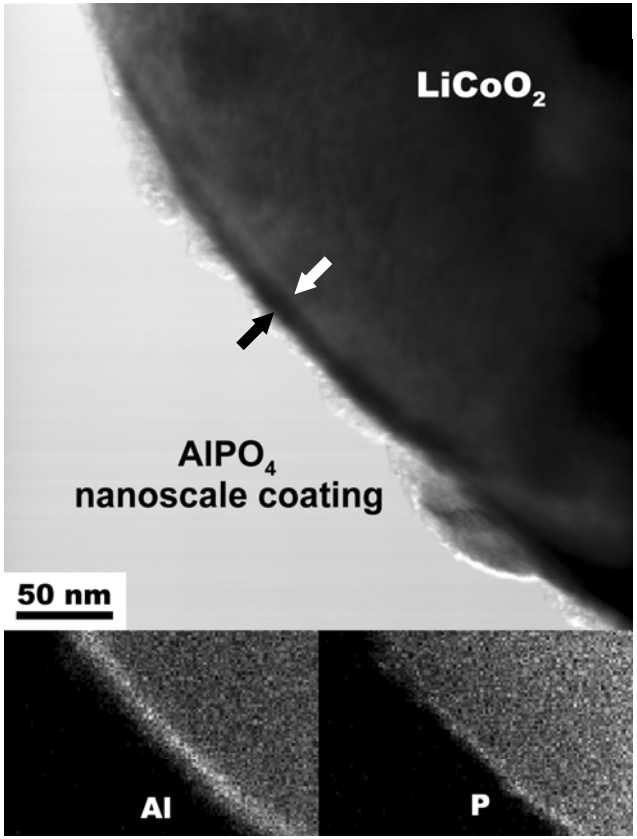

TEM bright-field image of the $AlPO_4$ nanoparticle-coated $LiCoO_2$; EDS confirms the Al and P components in the coating layer.

EDS confirms the Al and P components in the nanoscale-coating layer.

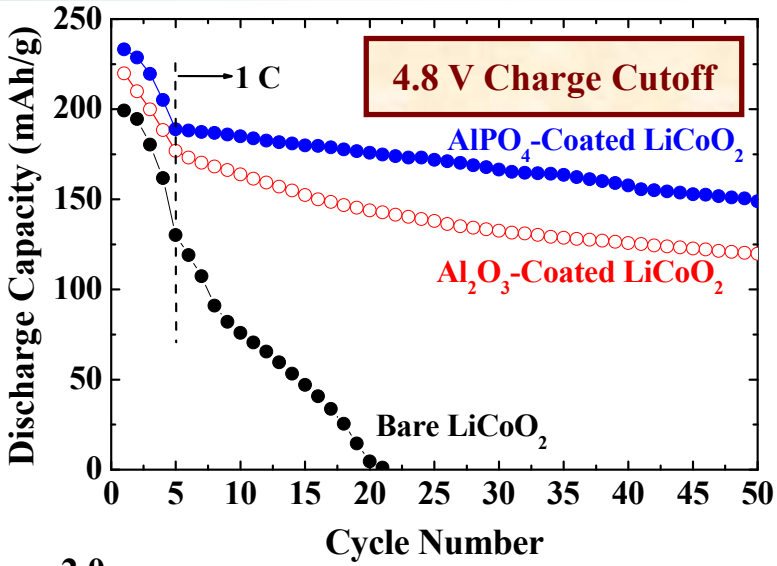

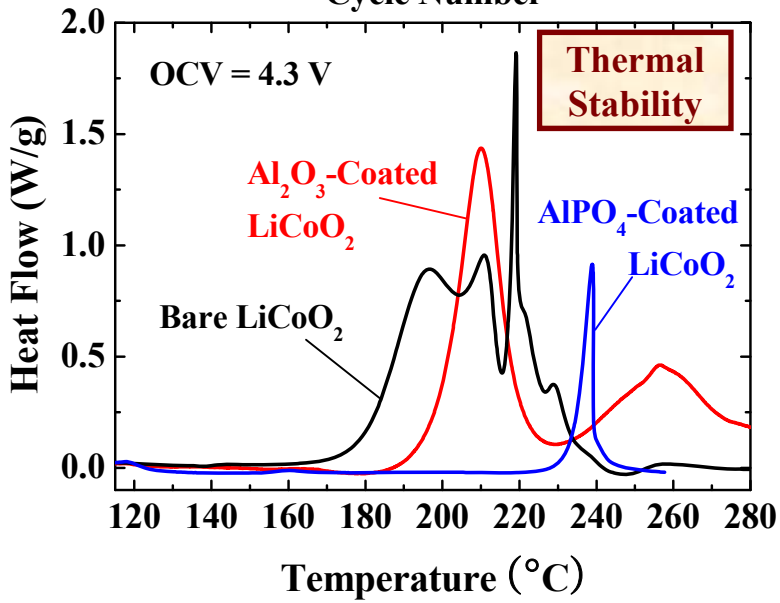

➢ B. Park's group, *Angew. Chem. Int. Ed.* (2003).

➢ B. Park's group, *J. Power Sources* (2005).

Sample Preparation

Metal-Oxide Coating

$M(OOC_8H_{15})_2(OC_3H_7)_2$

Isopropanol (Flammable)

$AlPO_4$-Nanoparticle Coating

$Al(NO_3)_3 \cdot 9H_2O$ + $(NH_4)_2HPO_4$

Distilled Water

Mixing with $LiCoO_2$ Powders (~10 μm in diameter)

Drying at 130°C and firing at 700°C for 5 h

$AlPO_4$-Nanoparticle Solution

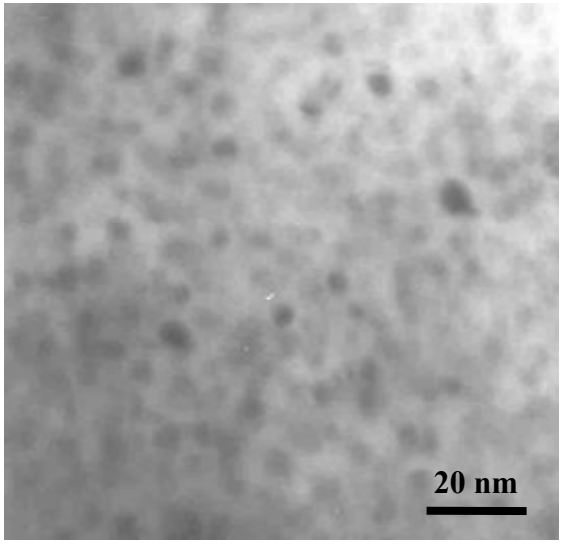

- **$AlPO_4$-Nanoparticle Coating**
  - Continuous Coating Layer
  - Easy Control (shape, size, coating thickness)

Charge-Discharge Tests

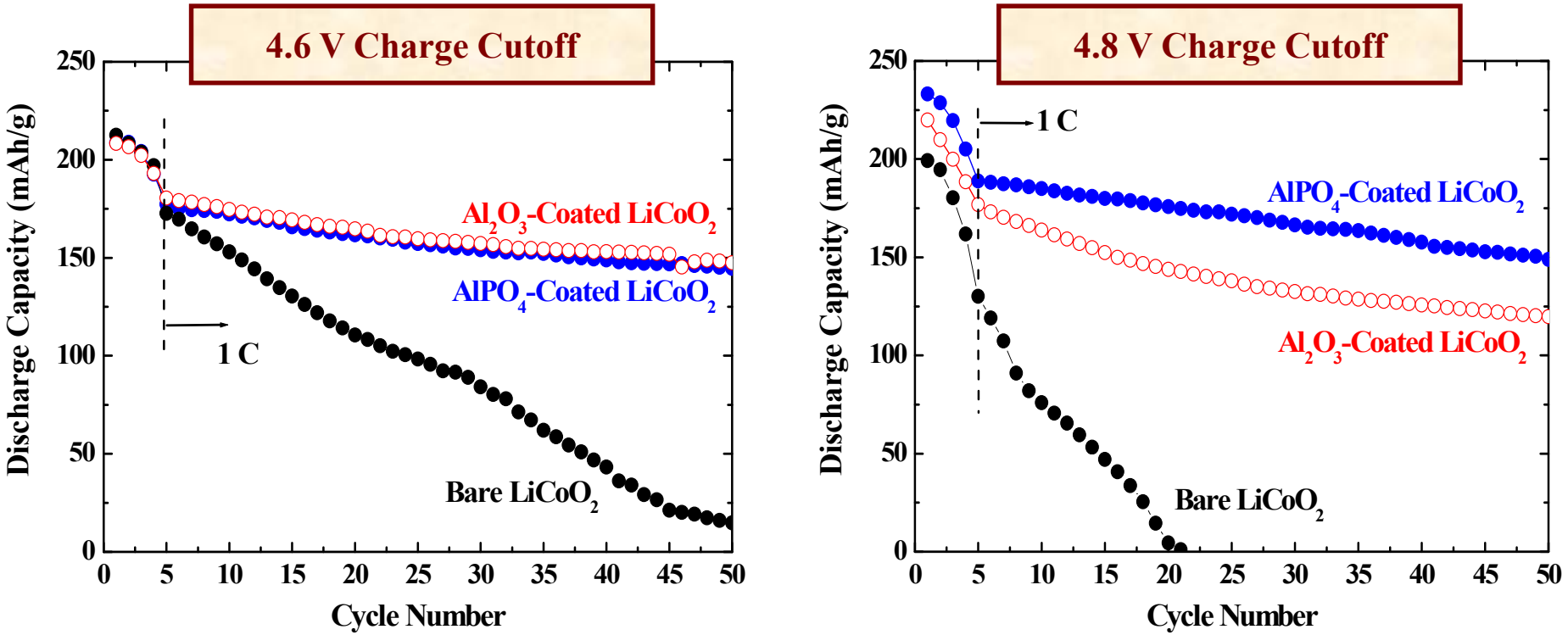

$AlPO_4$-coated $LiCoO_2$ is very stable at the high-charged state.

- J. Cho, T.-G. Kim, C. Kim, J.-G. Lee, Y.-W. Kim, and B. Park *J. Power Sources* **146**, 58 (2005).

Coating-Thickness Effect

Bare $LiCoO_2$

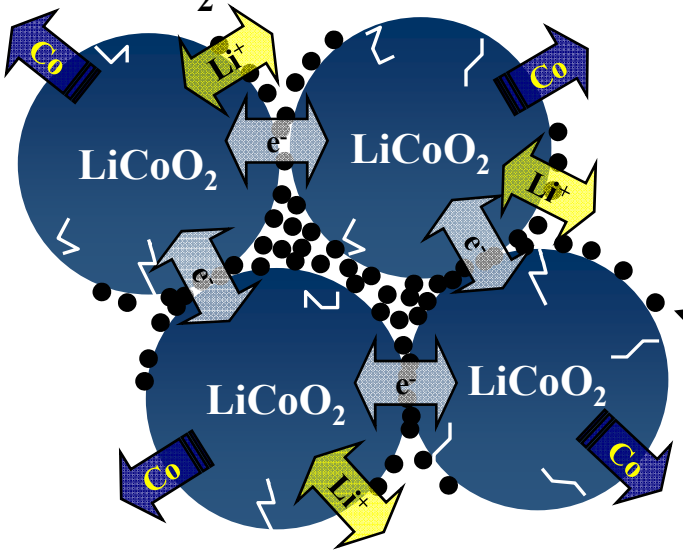

Thin coating

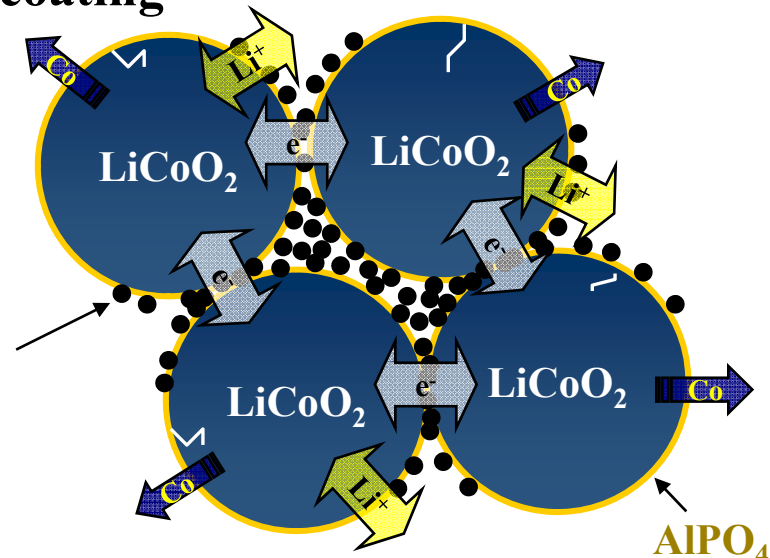

Carbon Black

$AlPO_4$

Thick coating

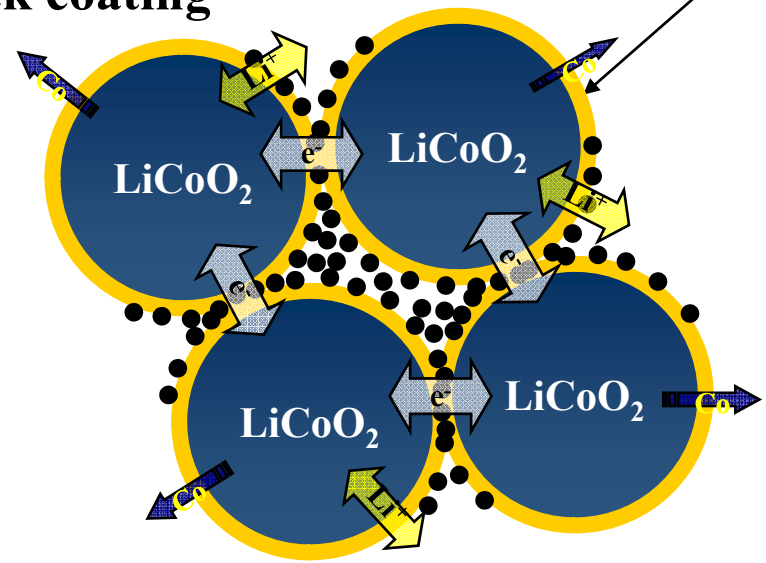

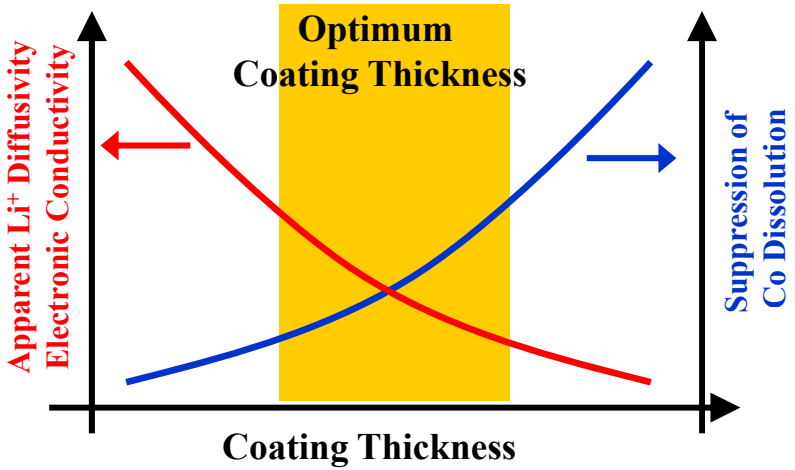

Below 1.0 wt. %-coated $LiCoO_2$?

Spin Coating of $AlPO_4$ Nanoparticles with Various Nanostructures

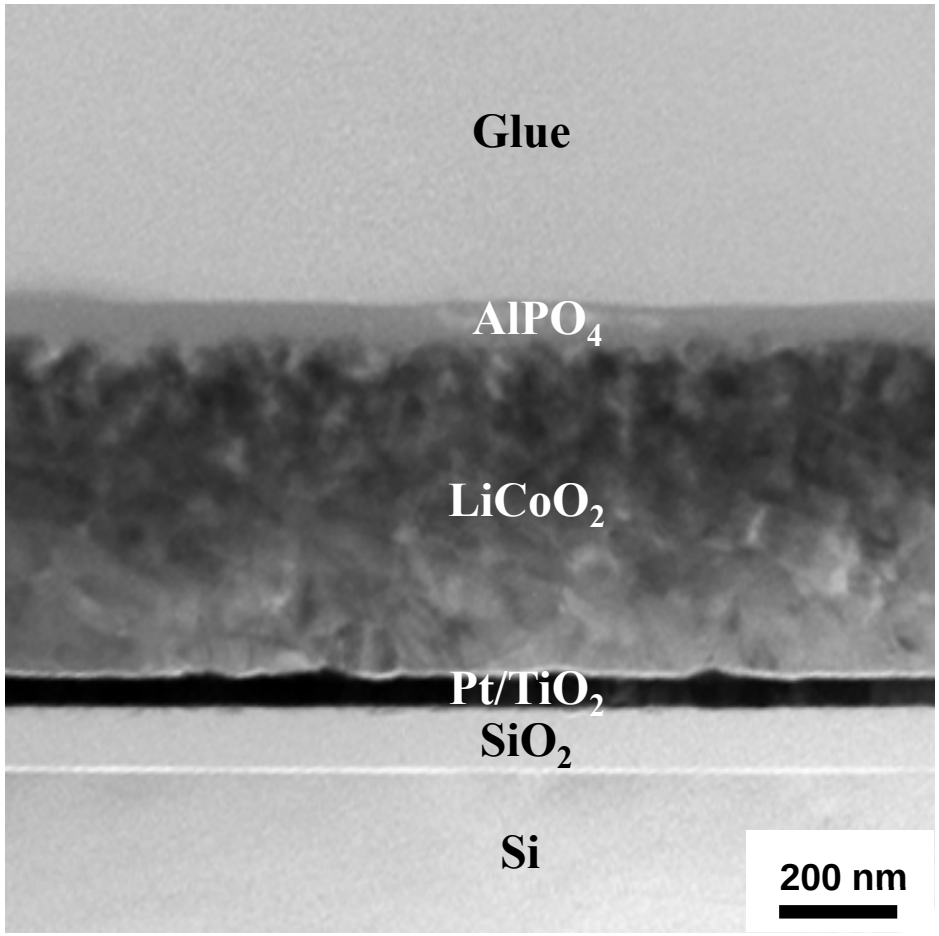

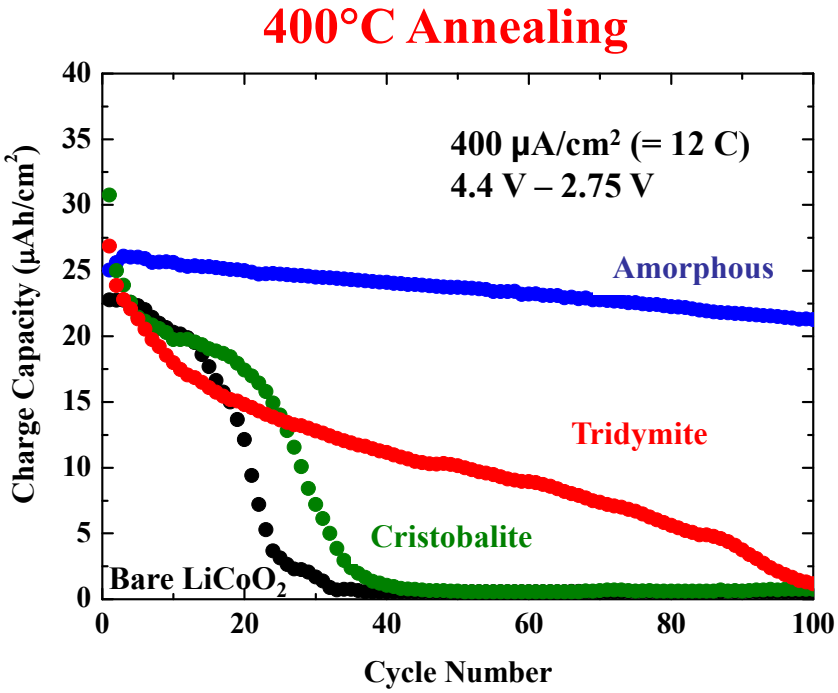

Optimum Nanostructures?

TEM confirms the uniform coating layer on $LiCoO_2$ thin film.

- B. Kim, C. Kim, D. Ahn, T. Moon, J. Ahn, Y. Park, and B. Park, *Electrochem. Solid-State Lett.* **10**, A32 (2007).

SnO_2 Nanoparticles

SnO_2 Nanoparticles: Mechanisms and Synthesis

Problems of SnO_2 Electrode

- Severe capacity loss by volume change between Li_xSn and Sn phases (~300%).
- Particles become detached and electrically inactive.

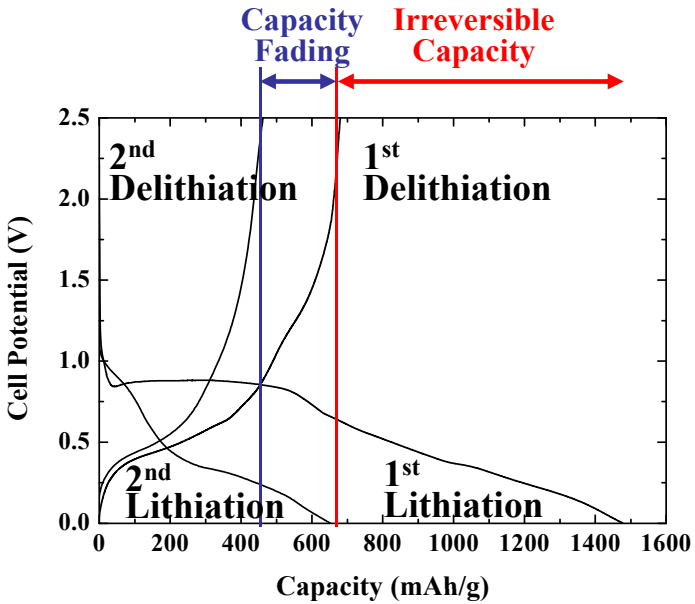

Voltage Profile of ~10 ㎛ SnO_2

- T.-J. Kim, D. Son, J. Cho, B. Park, and H. Yang *Electrochim. Acta* **49**, 4405 (2004).

SnO_2 Nanoparticles: Effective Solution

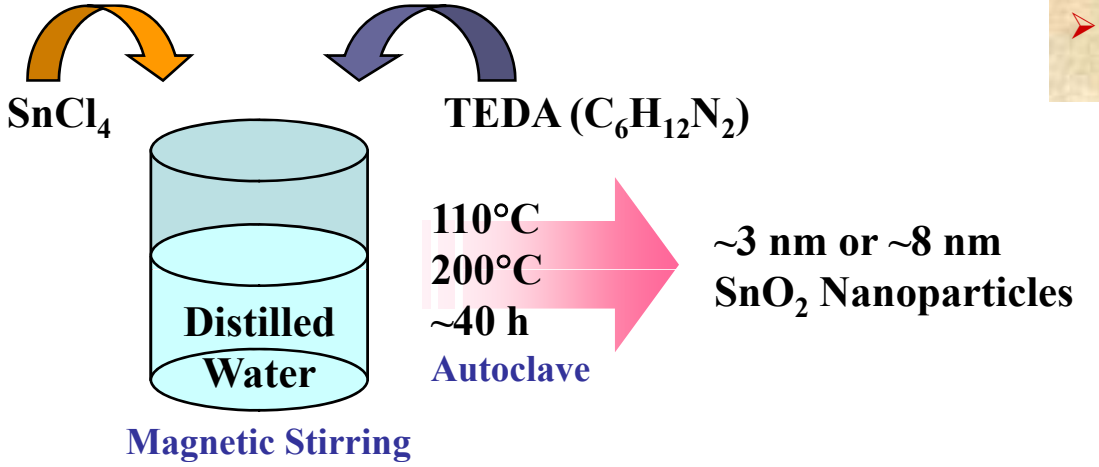

1st Lithiation:

$$8.4Li + SnO_2 \rightarrow 2Li_2O + Li_{4.4}Sn$$

~1490 mAh/g

1st Delithiation:

$$4.4Li + Sn \leftarrow Li_{4.4}Sn$$

~780 mAh/g

SnO_2-Nanoparticle Anode with Different Particle Sizes

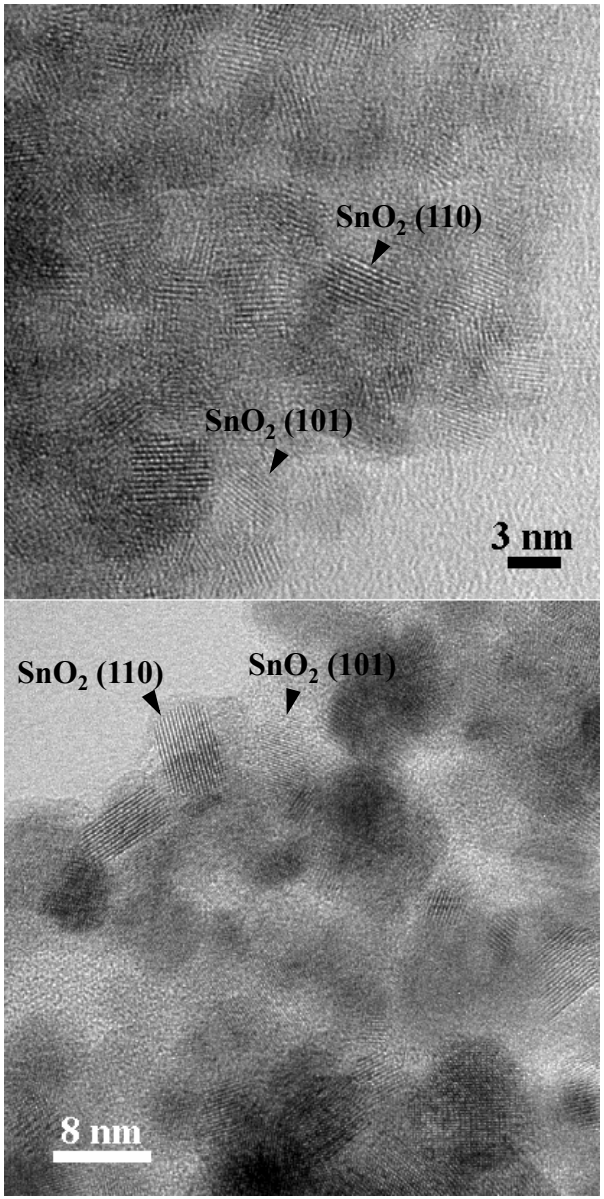

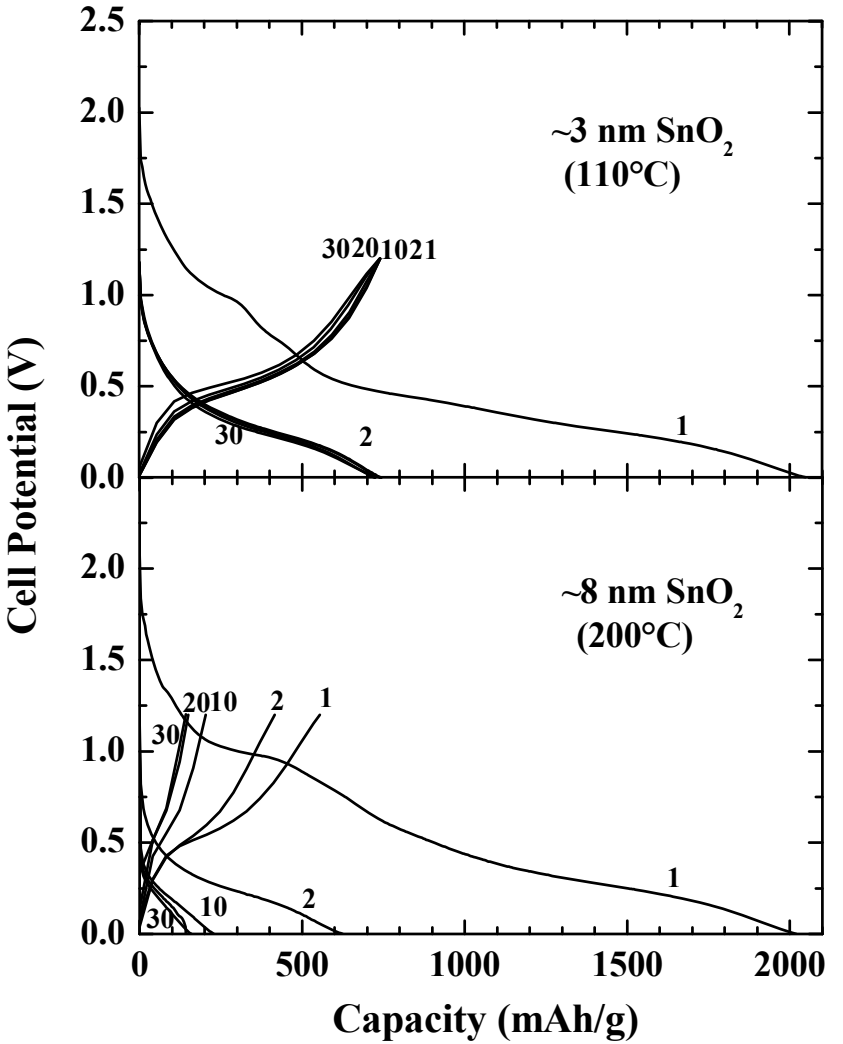

➢ C. Kim, M. Noh, M. Choi, J. Cho, and B. Park *Chem. Mater.* **17**, 3297 (2005).

Carbon-Coated SnO_2 Nanoparticles: Synthesis

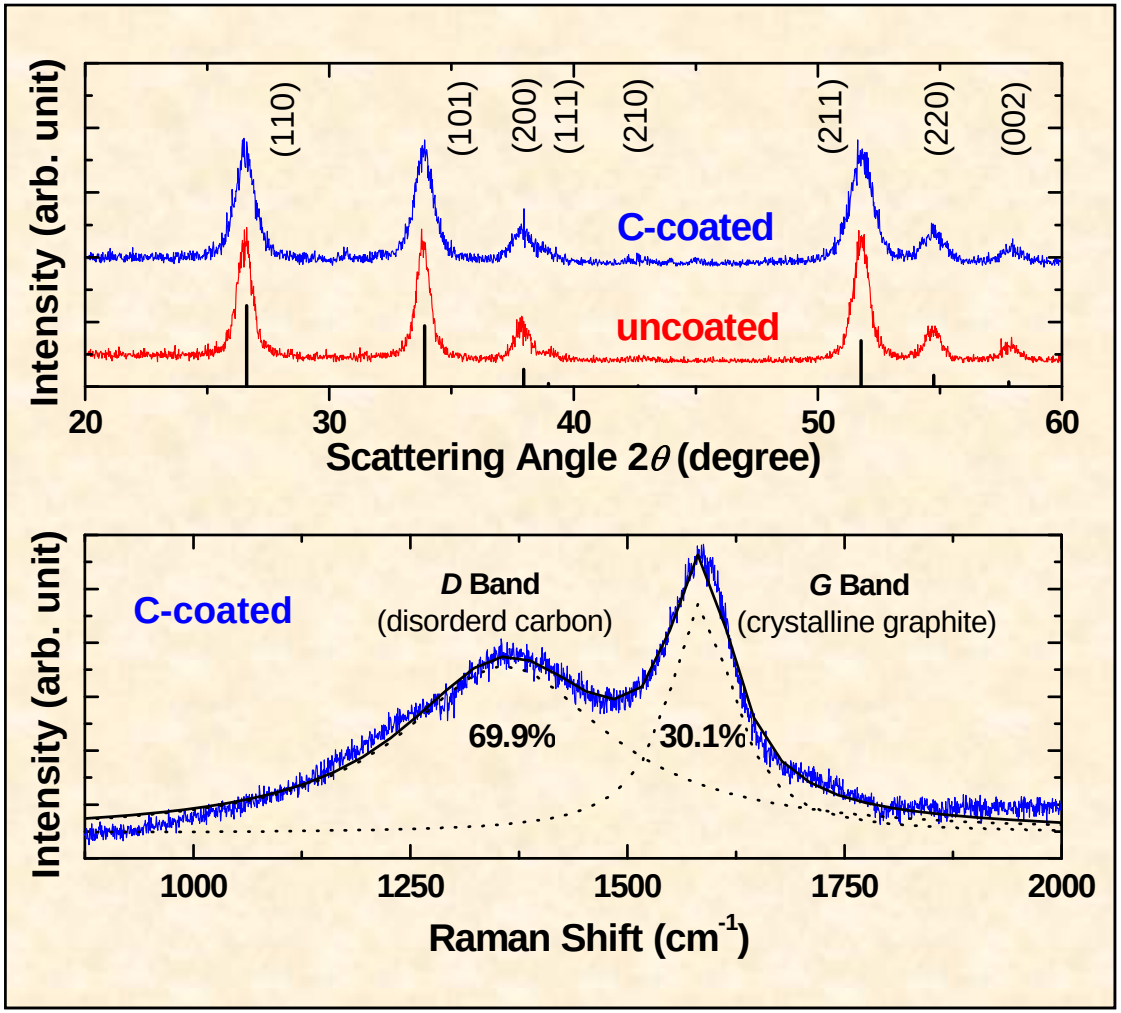

Disordered-carbon-coated SnO_2 nanoparticles

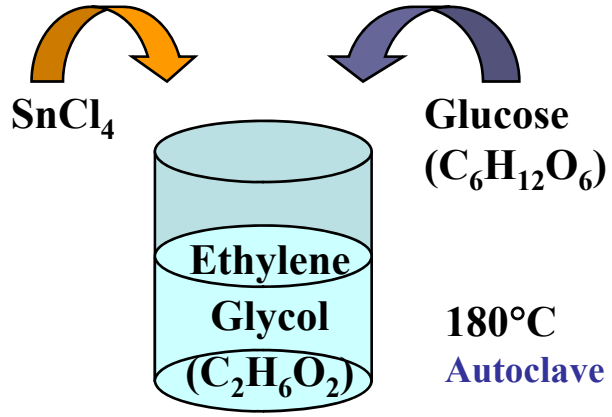

500°C Carbonization → **Carbon-Coated SnO_2 Nanoparticles**

	Size	Local Strain
C-coated	8.8 ± 0.9 nm	0.59 ± 0.13%
uncoated	13.2 ± 1.1 nm	0.13 ± 0.08%

	SnO_2 (wt. %)	C (wt. %)	H (wt. %)
C-coated	90	4.9	0.35
uncoated	97	0.061	0.074

by ICP

Carbon-Coated SnO_2 Nanoparticles

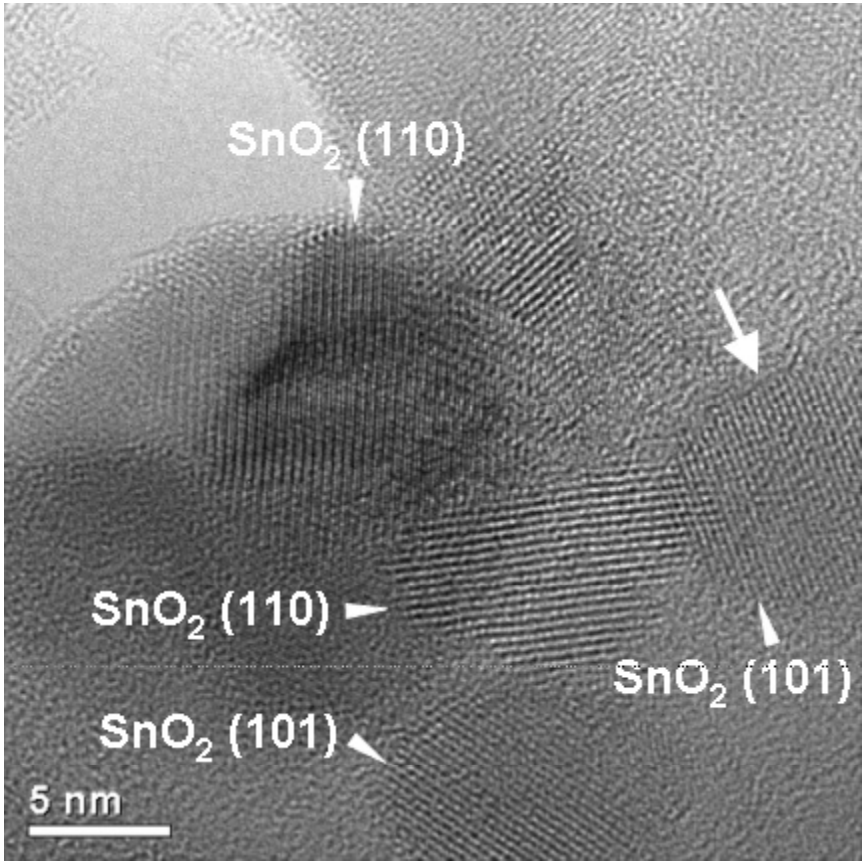

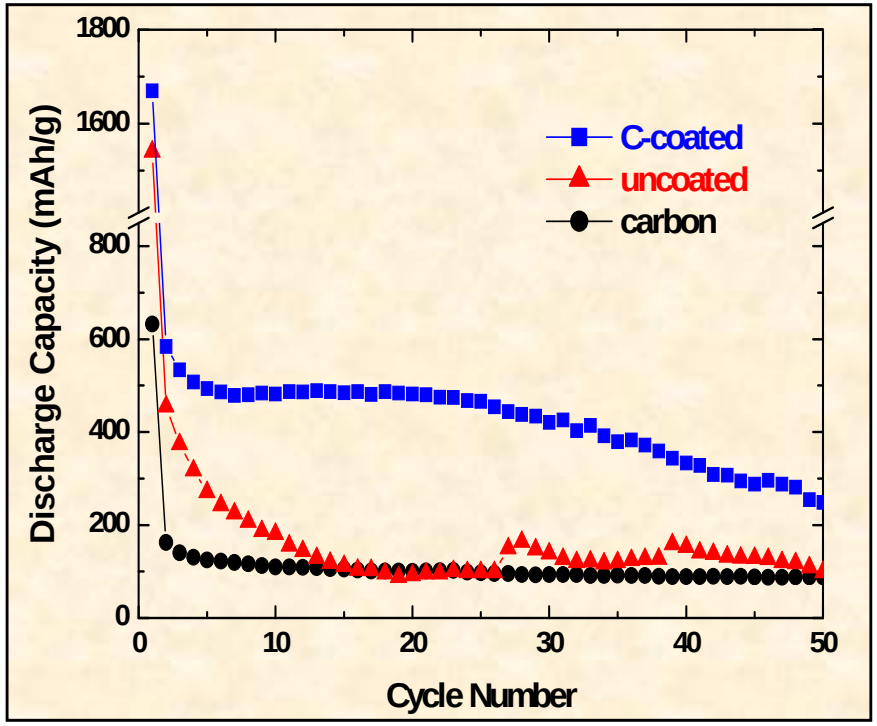

➢ T. Moon, C. Kim, S.-T. Hwang, and B. Park *Electrochem. Solid-State Lett.* **9**, A408 (2006).

- **Most of the nanoparticles are well dispersed.**
- **SnO_2 nanoparticles are surrounded by disordered carbon. (graphite-interlayer spacing ≅ 0.35 nm)**
- **Capacity contribution of disordered carbon is ~10 mAh/g.**

Mesoporous Tin Phosphate

Tin-Phosphate Anodes

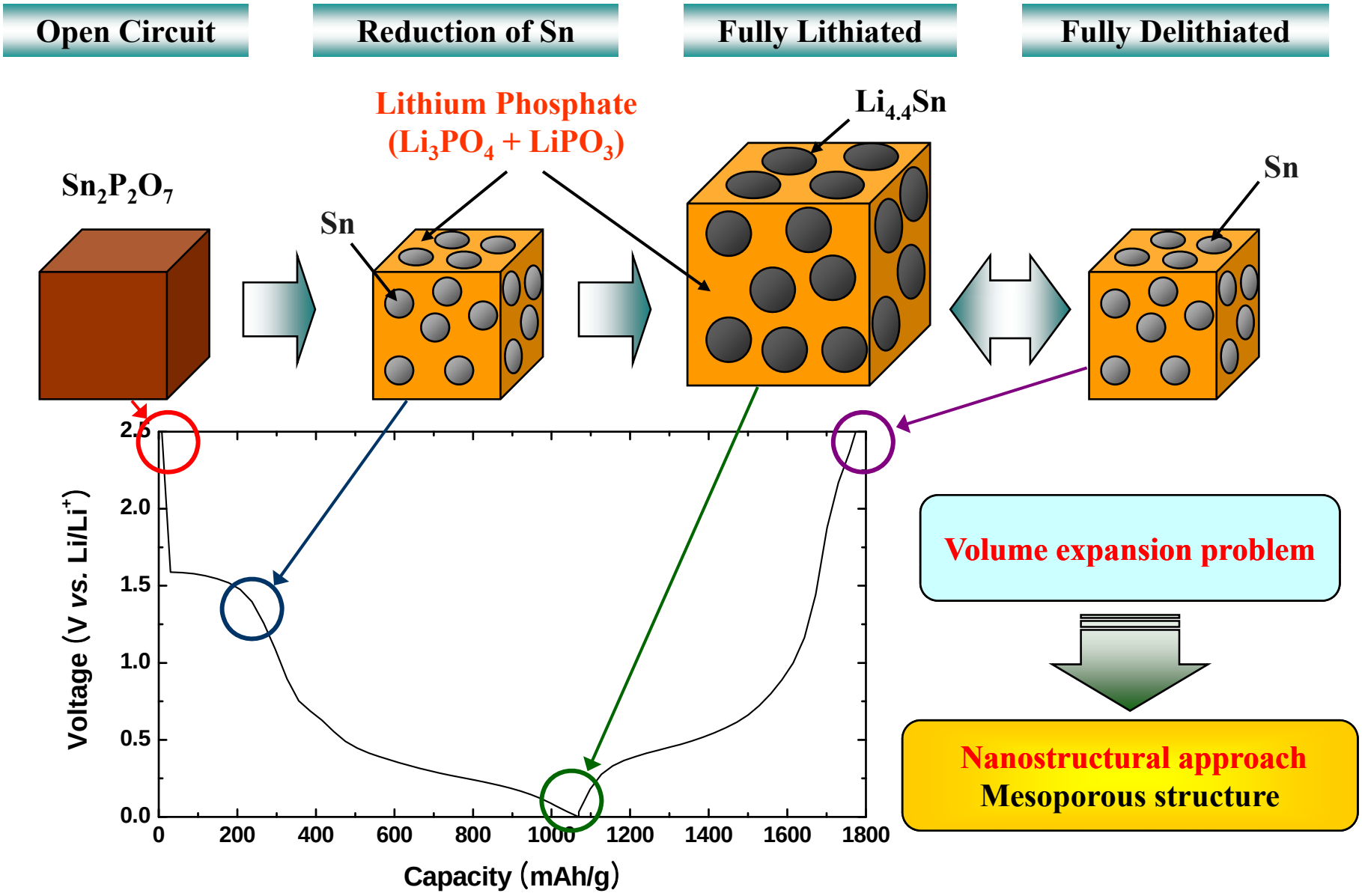

Mesoporous Materials

Mesoporous material:
- **Inorganic solids with pore diameters of 2 – 50 nm**
- **Long-range ordering of pores**

Hexagonal **Cubic** **Layered**

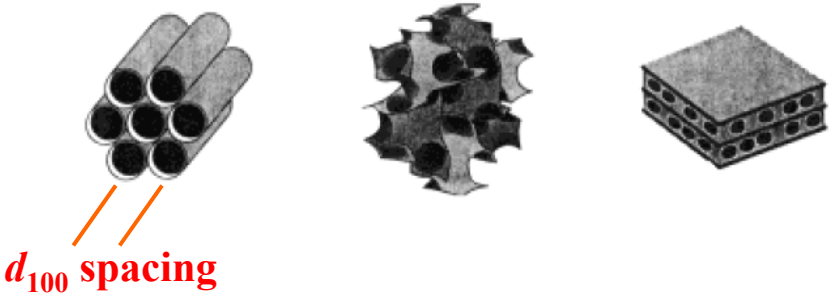

➢ J. Y. Ying's group (MIT), *Angew. Chem. Int. Ed.* (1999).

TEM Images of Hexagonal Mesoporous Silica

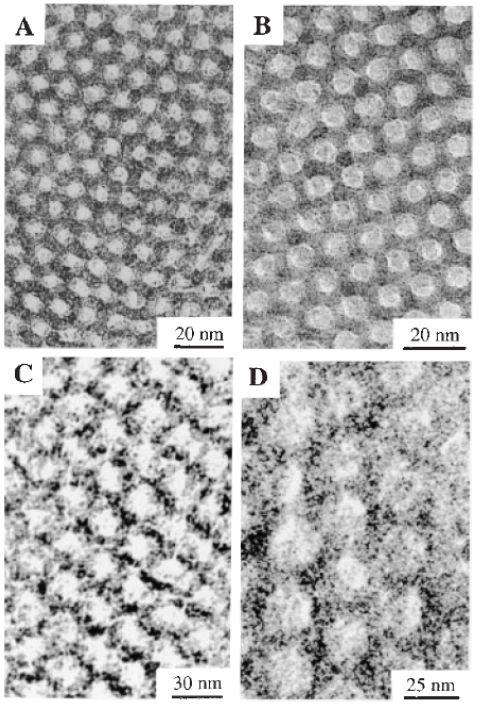

TEM images of calcined hexagonal SBA-15 mesoporous silica with different average pore sizes, from BET and XRD results (*24*): (**A**) 60 Å, (**B**) 89 Å, (**C**) 200 Å, and (**D**) 260 Å. The thicknesses of the silica walls are estimated to be (A) 53 Å, (B) 31 Å, (C) 40 Å, and (D) 40 Å. The micrographs were recorded digitally with a Gatan slow-scan charge-coupled device (CCD) camera on a JEOL 2010 electron microscope operating at 200 kV. The samples were prepared by dispersing the powder products as a slurry in acetone, which was then deposited and dried on a holey carbon film on a Cu grid. A low-exposure technique was used to reduce the effect of beam damage and sample drift. Focus-series measurements show that the bright areas correspond to the pores and dark areas to the silica walls.

➢ G. D. Stucky's group (UC Santa Barbara), *Science* (1998).

Mesoporous Materials

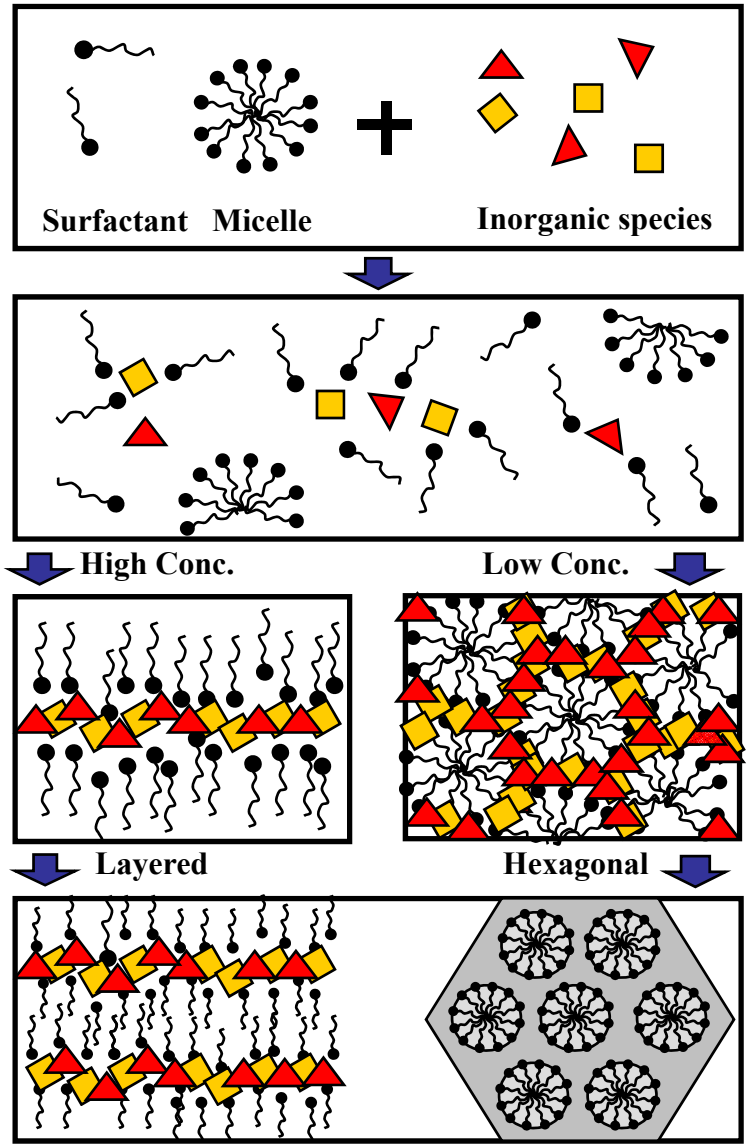

Reaction of single-chain surfactants with inorganic polyanions

Nucleation and precipitation of organized arrays

Condensation with time and temperature

➢ G. D. Stucky's group (UC Santa Barbara)
Chem. Mater. (1994).

Synthesis of Mesoporous Tin Phosphates

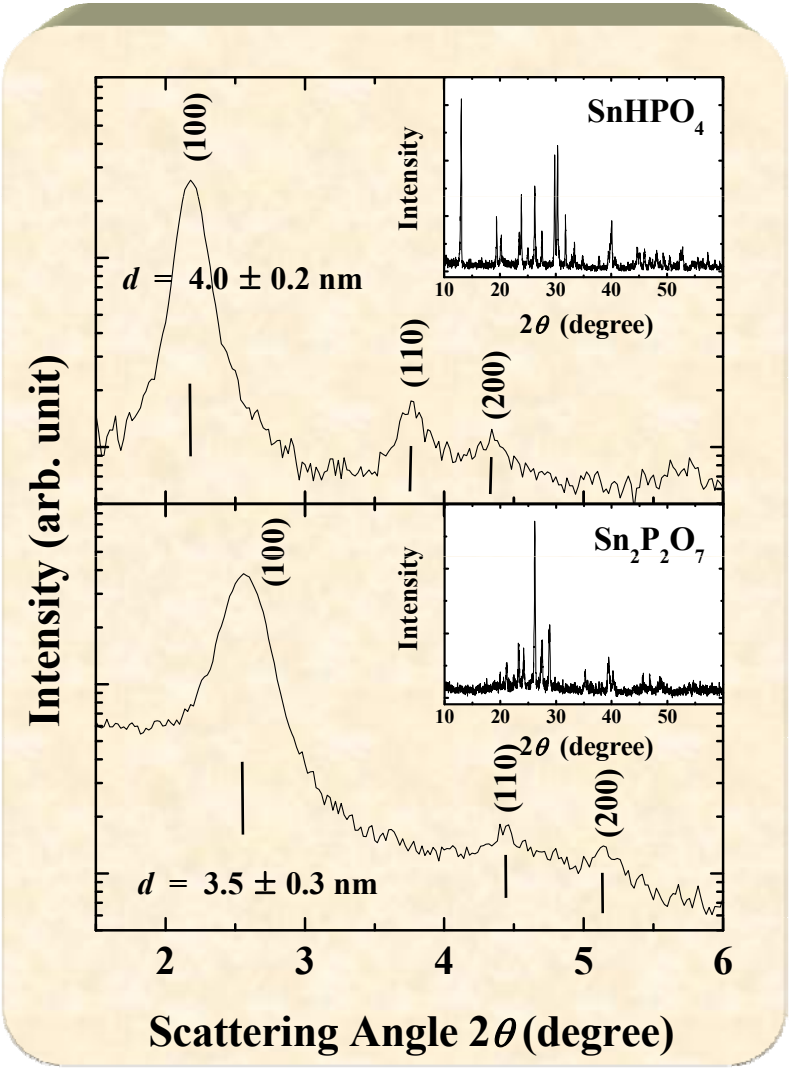

SnF_2 and H_3PO_4 dissolved in distilled water
+
CTAB $(CH_3(CH_2)_{15}N(CH_3)_3Br)$
90°C Aging

As Synthesized
Mesoporous Tin Phosphate / $SnHPO_4$

400°C Calcination
Mesoporous Tin Phosphate / $Sn_2P_2O_7$

Hexagonal Mesostructure

➢ B. Park's group, *Angew. Chem. Int. Ed.* (2004).

Mesoporous Tin Phosphates

TEM Images

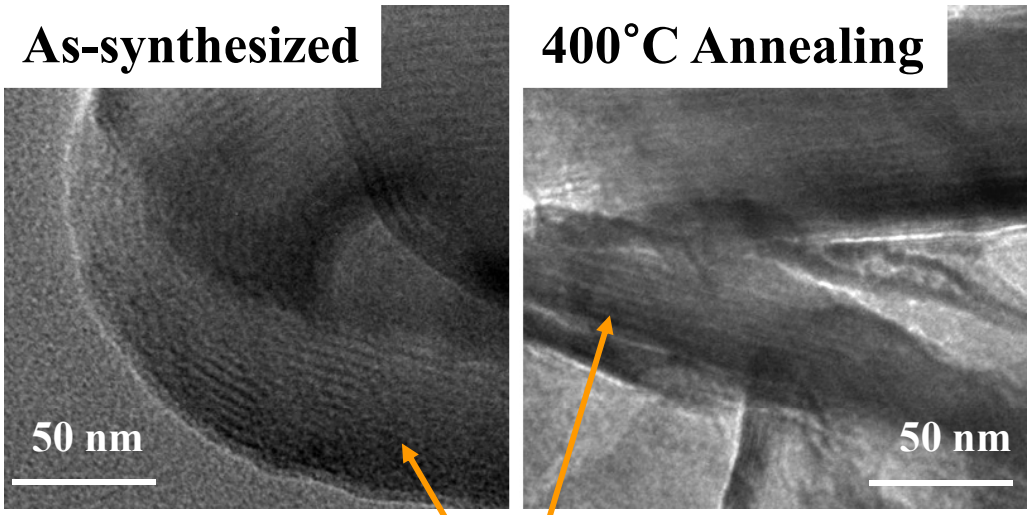

***d* spacing: ~3.8 nm** **d spacing: ~3.3 nm**

Mesopore channel (bright stripes)
Tin phosphate wall (dark stripes)

Electrochemical Properties

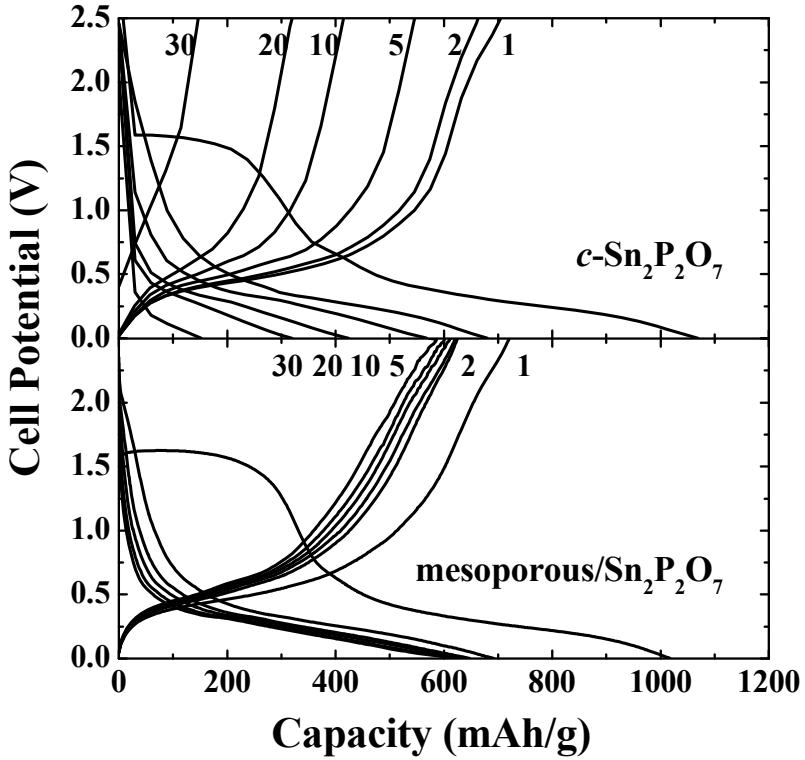

Novel Mesoporous/Crystalline Composite:
– **High initial charge capacity (721 mAh/g)**
– **Excellent cycling stability**
(among the tin-based anodes)

➢ B. Park's group, *Angew. Chem. Int. Ed.* (2004).

Change of Mesoporous Structure during Charge/Discharge

The Corresponding *d* Spacing

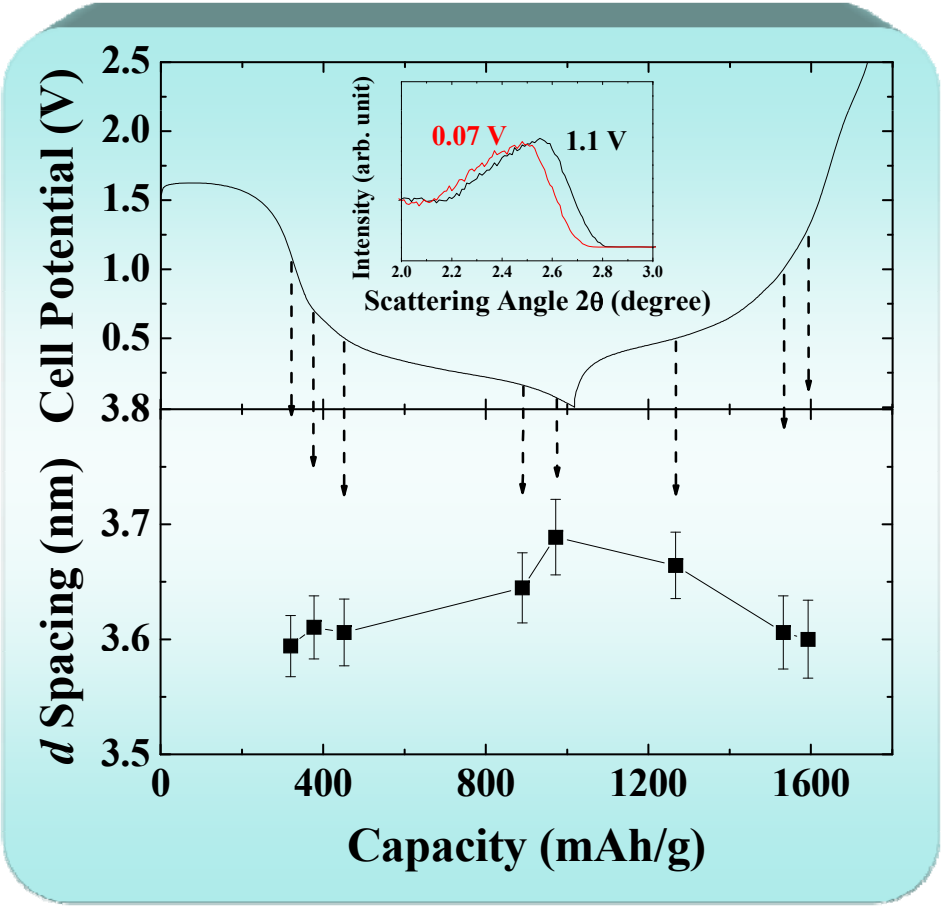

▶ **The *d* spacing expands and shrinks with Li alloying/dealloying.**

▶ **The mesopores do not collapse during the 1st discharge and charge.**

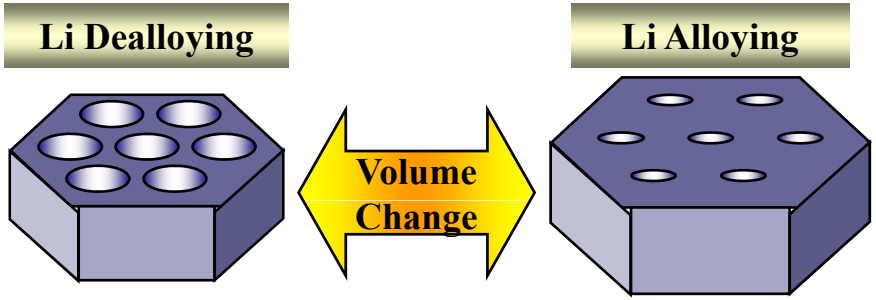

Mesopore ratio (mesoporous: non-mesoporous tin phosphate) ≈ 1 : 3

Control of Mesopore Ratio
(Surfactant/Precursor Ratio)

Characterization of Mesoporous Structures

Small-Angle XRD Patterns

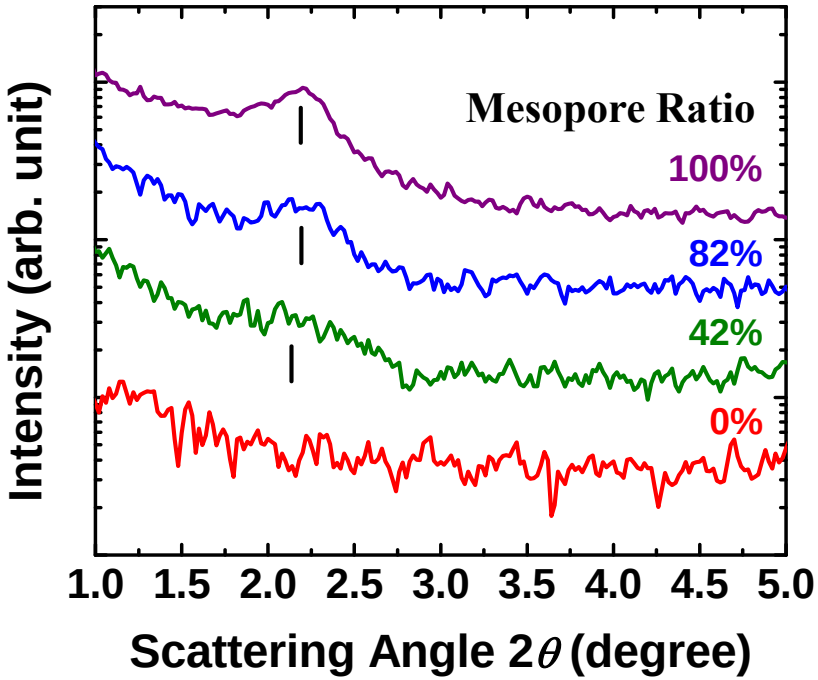

N_2-Adsorption/Desorption Isotherms

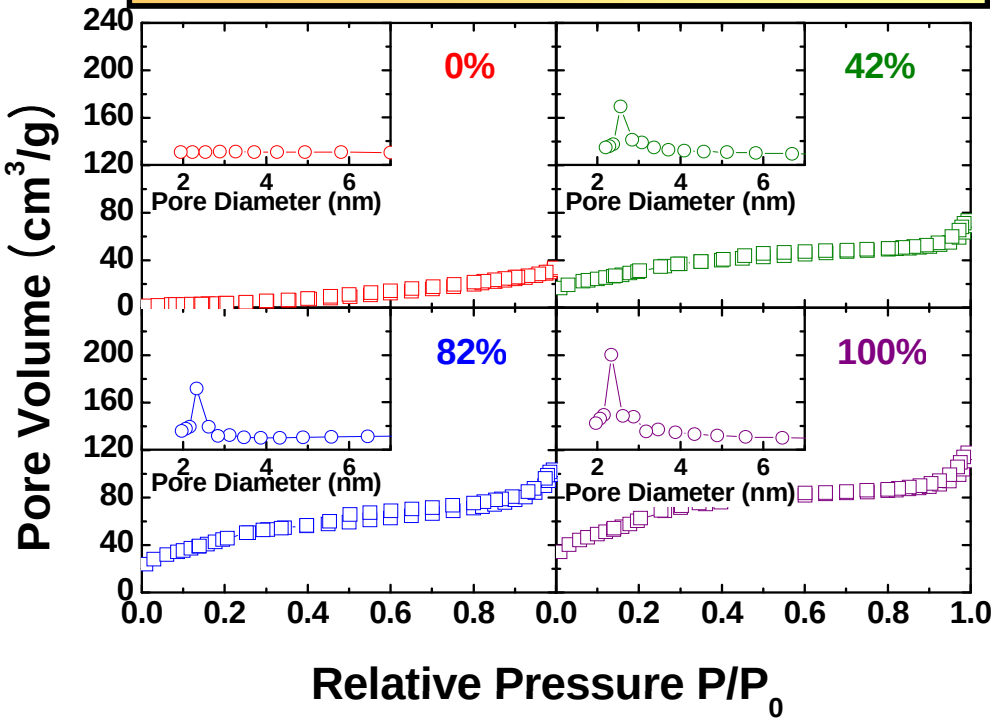

Precursor Molar Ratio	Mesopore *d* Spacing (nm)	Average Pore Size (nm)	BET Surface Area (m^2/g)	Relative Mesopore Ratio	Composition of Synthesized
0.11	—	—	15	0%	$Sn_{1.94}P_2O_{7.3}$
0.22	4.29 ± 1.21	2.56	114	42%	$Sn_{2.30}P_2O_{7.5}$
0.54	4.34 ± 0.68	2.32	167	82%	$Sn_{2.61}P_2O_{7.8}$
1.10	4.20 ± 0.63	2.33	221	100%	$Sn_{2.77}P_2O_{8.1}$

Tridymite $FePO_4$ in the Low Voltage Range

High Reactivity of Metallic Nanoparticles

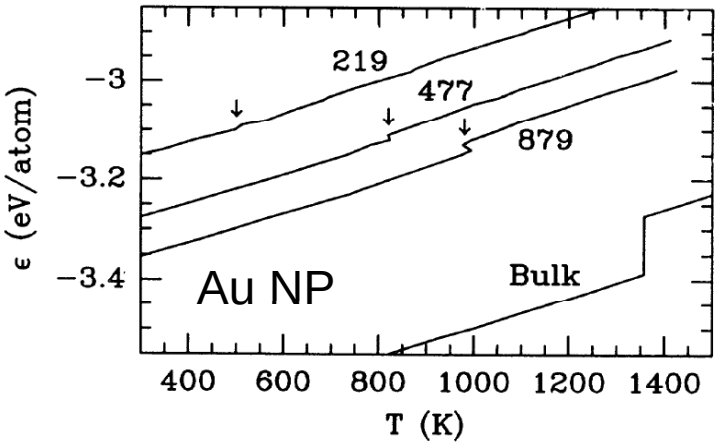

F. Ercolessi et al.
IBM Zurich, Phys. Rev. Lett. (1991)

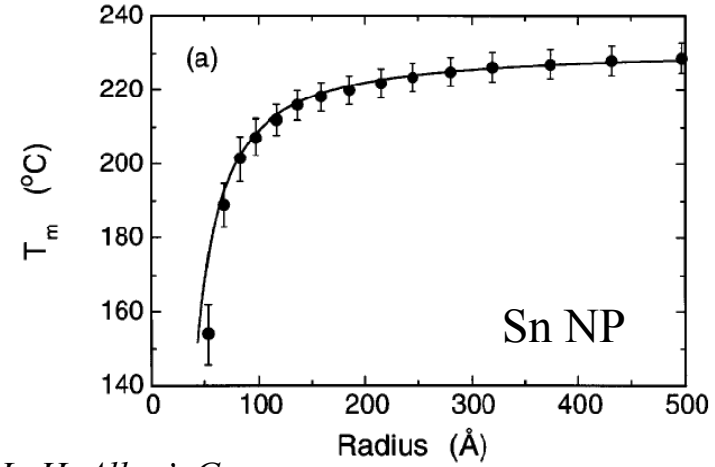

L. H. Allen's Group
UIUC, Phys. Rev. Lett. (1996)

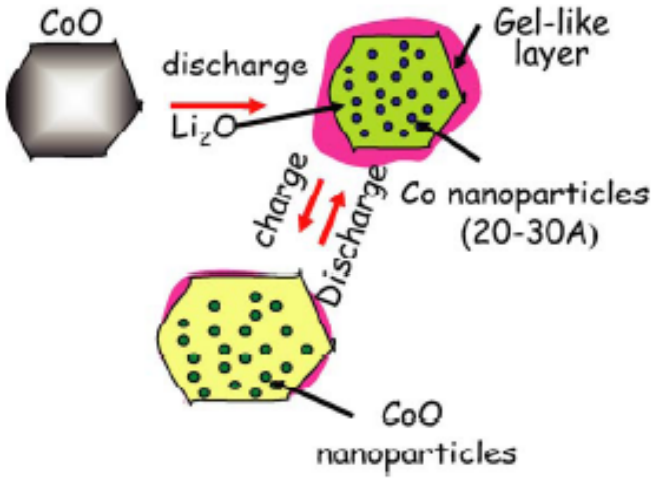

$M_xO_y + 2yLi^+ + 2ye^- \leftrightarrow yLi_2O + xM^0$

ex.) CoO, Cu_2O, FeO, NiO

J.-M. Tarascon's Group
U. Picardie Jules Verne, Nature (2000)

Nanoscale metallic nanoparticles show higher electrochemical reactivity than bulk

Electrochemical Reactivity of $FePO_4$ with Lithium

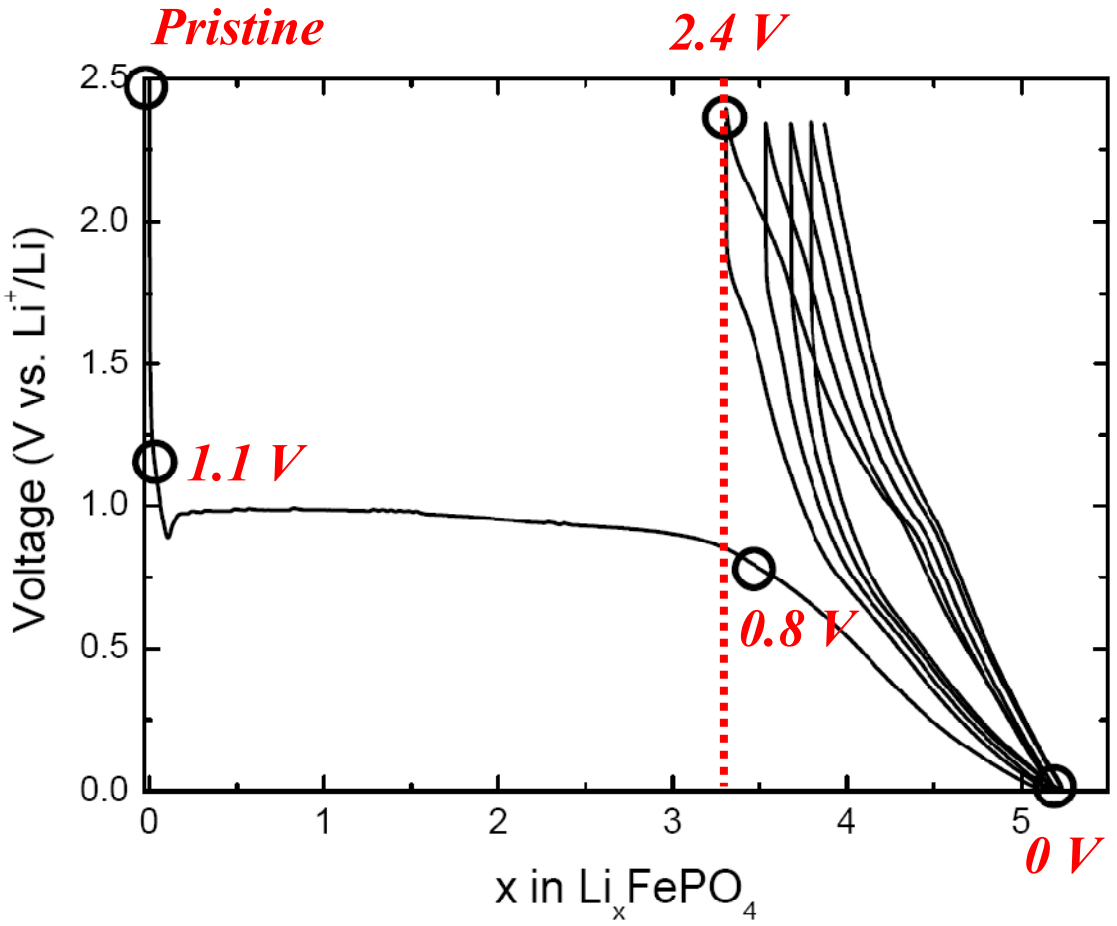

Investigation of Nanostructures with XAS, XRD, FT-IR, TEM, NMR, etc..
→ Revealing the reaction mechanisms of $FePO_4$ with Li

Phase Variation during Discharge and Charge

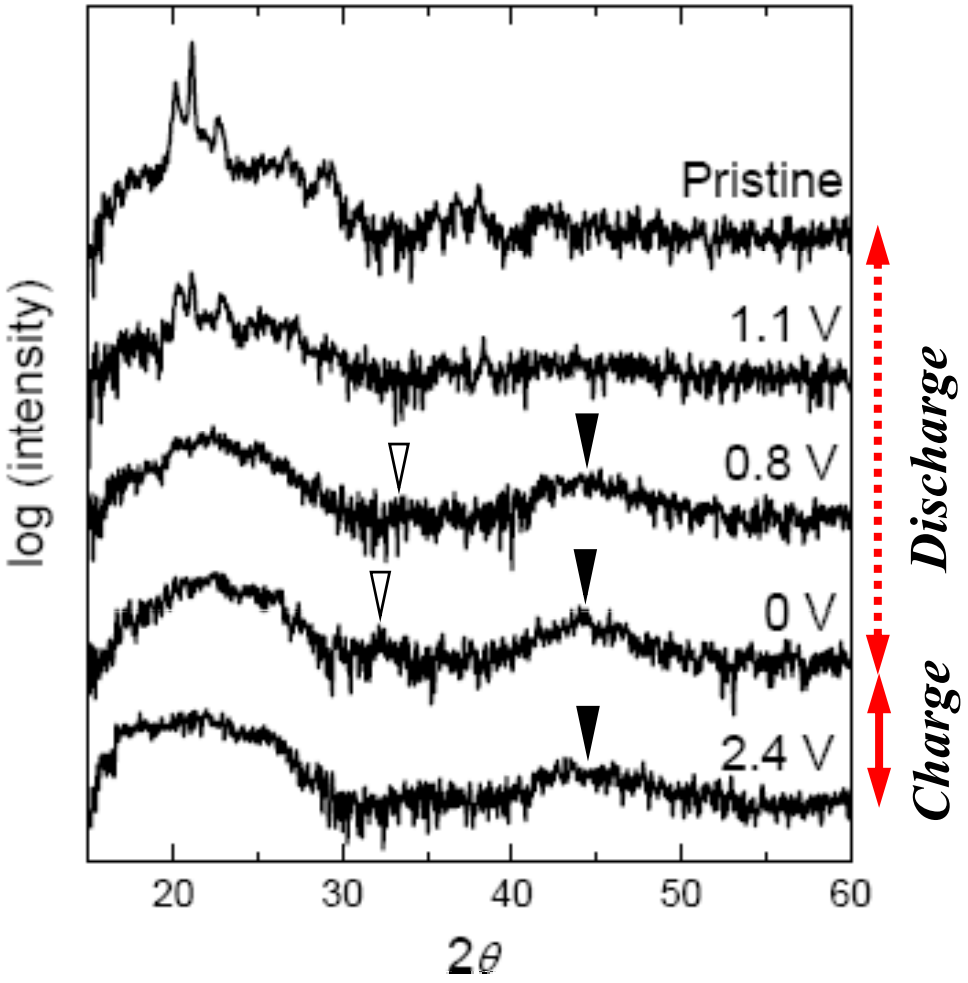

1. **Amorphization during discharge**
   - **not recovered during charge**

2. ▼ **: Fe metal (110) peak**
   - **~ 1 – 1.5 nm (*Scherrer* eq.)**
   - **slight decrease of intensity during charge**

   → *Fe redox reaction*

3. ▽ **: Li_2O (111) peak**
   - **lower shift during discharge**
   - **disappear after charge**

   → *Li_2O redox reaction*

Structural Variation during Discharge and Charge

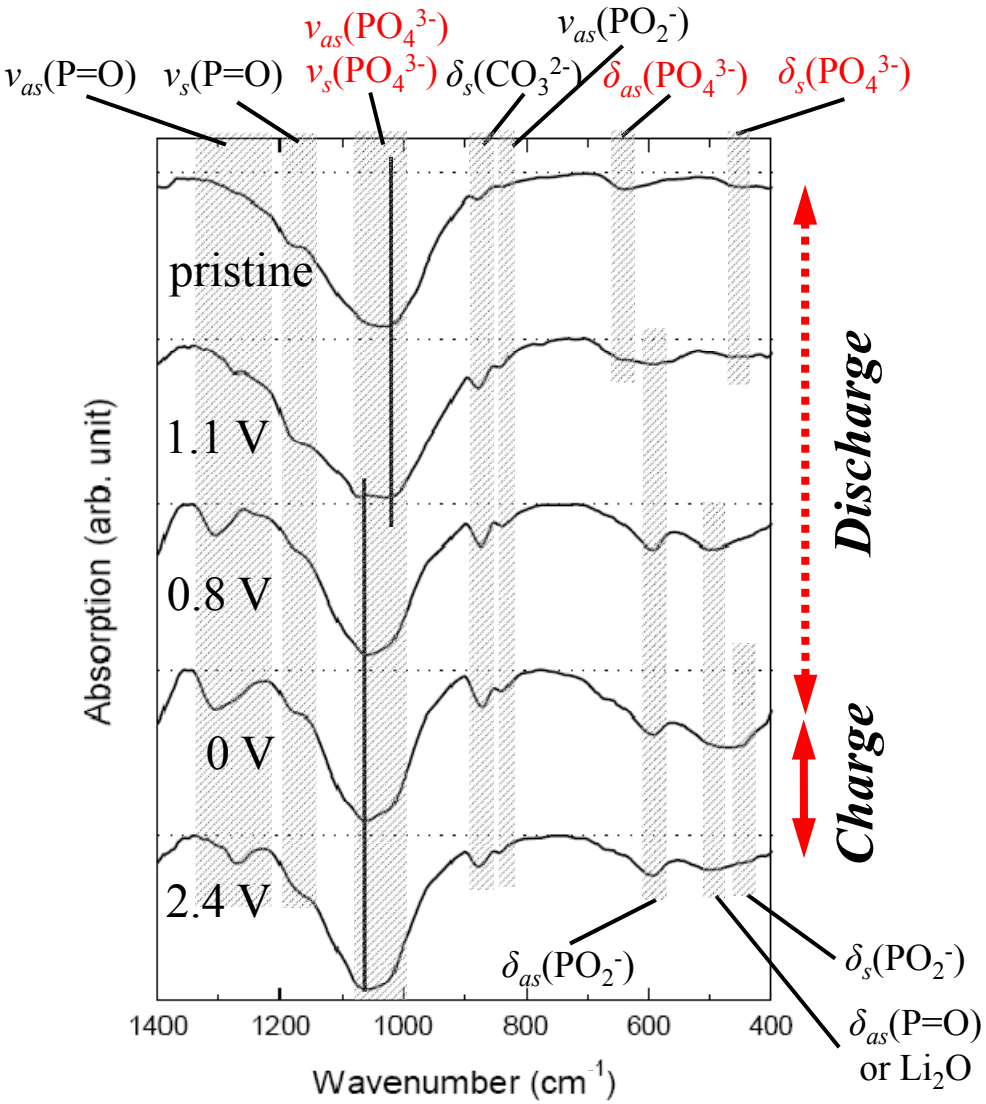

During discharge/charge process

- **PO_4 structure is sustained**
- **Fe-O-P changes to Li-O-P (Li_3PO_4 is formed)**
- **P=O and PO_2^- (defective bonds) structures are formed**
- **Li_2O seems to be formed**

TEM Investigation (Fully Discharged/Charged Sample)

Fully Discharged Sample (0 V)

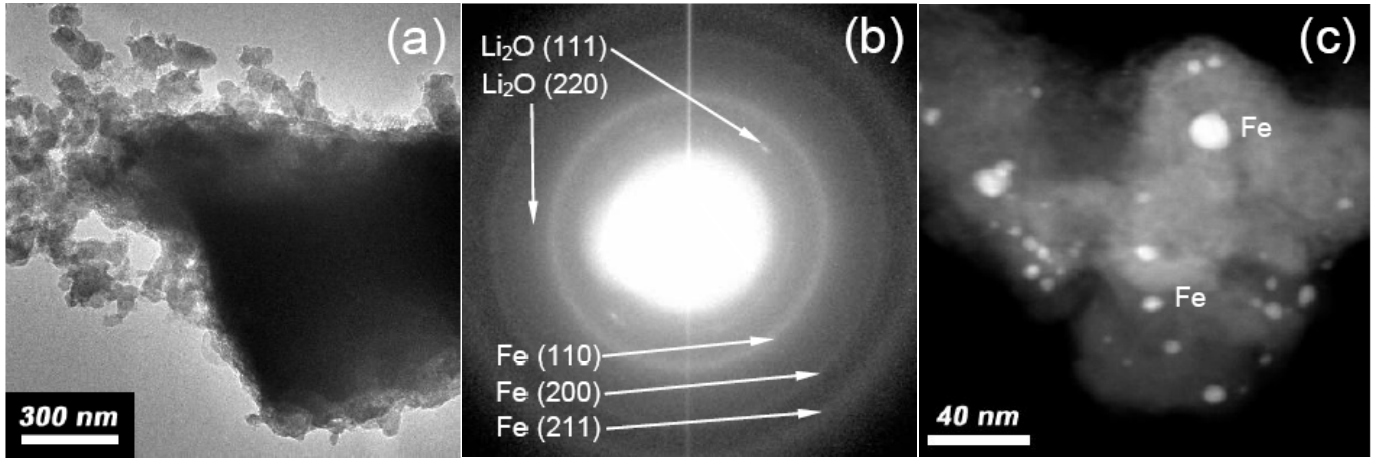

Fe nanoparticles in Li_2O matrix

Fully Charged Sample (2.4 V)

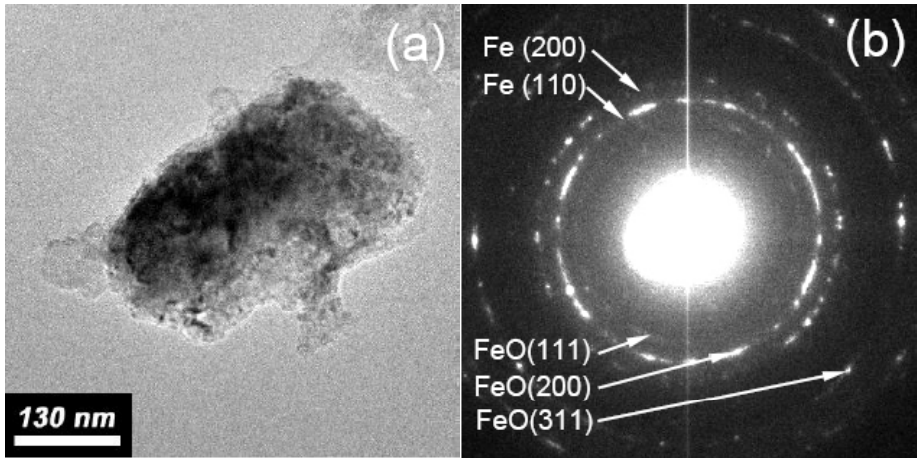

Coexistence of Fe and FeO

residual Fe:
Origin of small recovery

Valence Electron of Fe (XANES)

※From the sample with very small reversible capacity

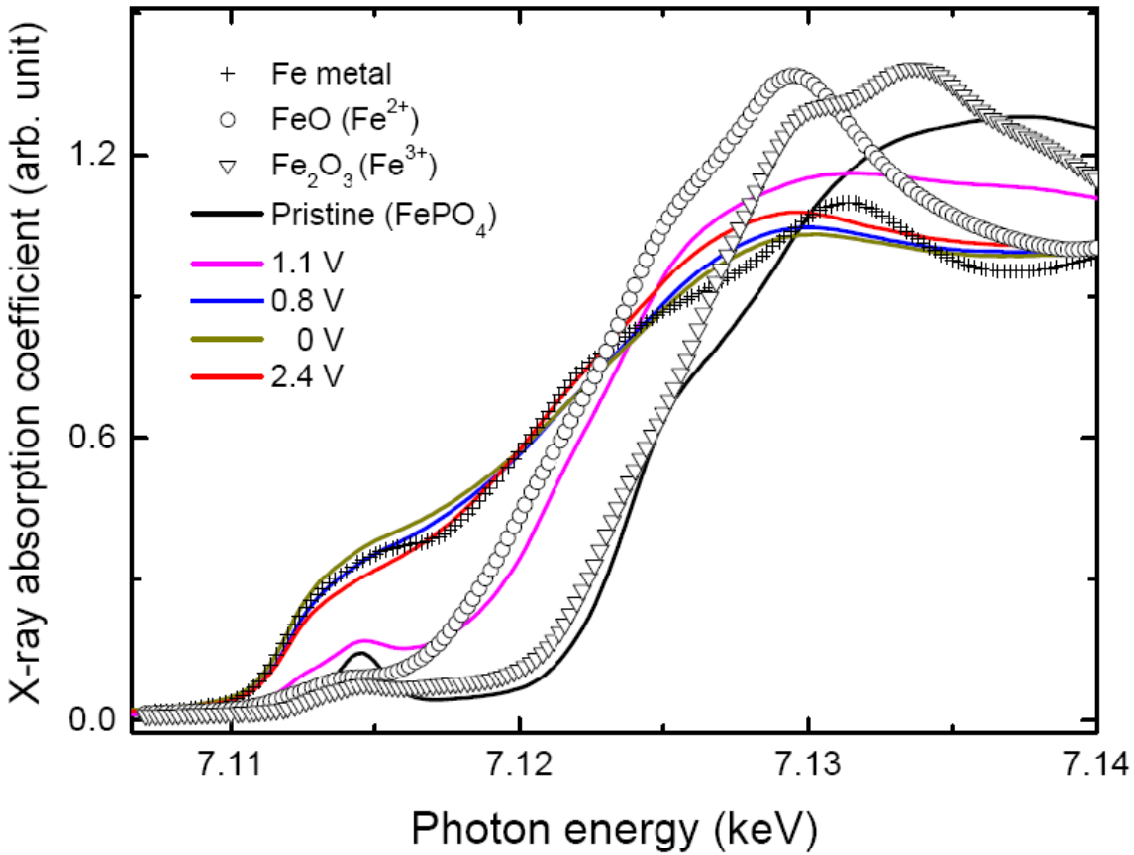

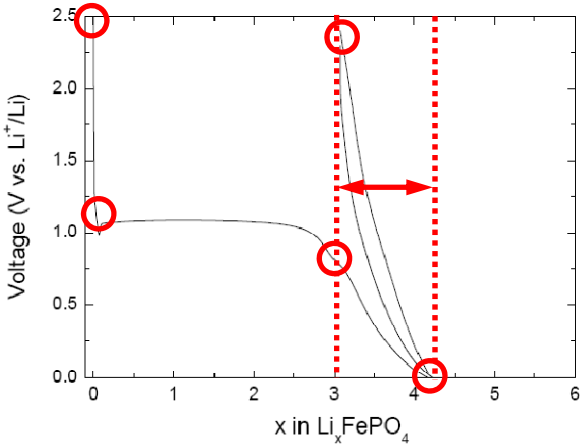

- **Change of valence # of Fe**
- **$FePO_4$ is almost discharged at 0.8 V**
- **Small recovery of valence # of Fe**

Radial Distribution Function for Fe (EXAFS)

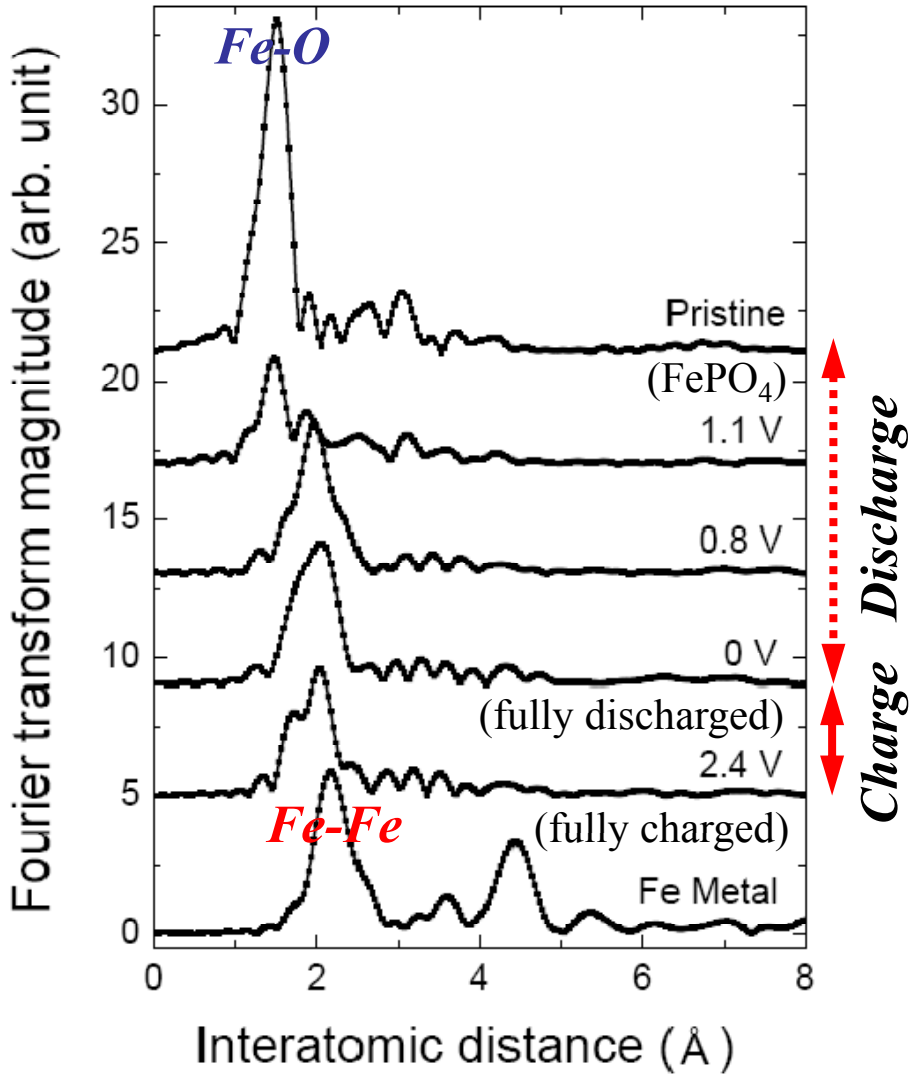

- **Pristine: well defined Fe-O (FeO_4-PO_4 structure)**
- **1.1 V : poorly defined Fe-O ($LiFePO_4$ structure)**
- **0.8 V : Fe-Fe (reduced Fe metal NP)**
- **0 V : Fe-Fe (reduced Fe metal NP)**
- **2.4 V : Fe-Fe and Fe-O mixed phase (residual Fe metal NP and FeO or Fe_2O_3)**

SnS_2 Nanosheet Anode Materials

Synthesis of SnS_2 Nanosheets

Synthesis of SnS_2 Nanosheets

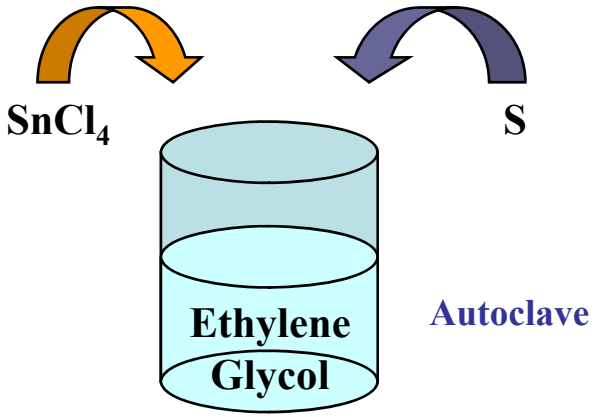

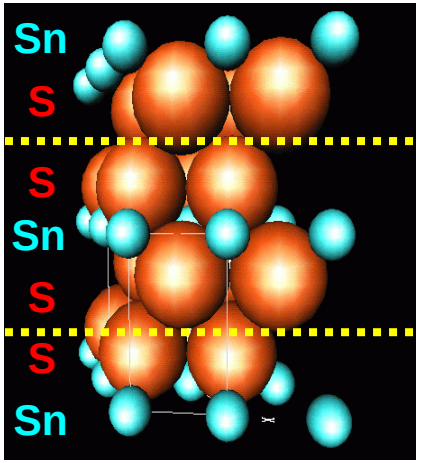

Layered Hexagonal ($P\bar{3}m1$)
(a = 3.648 Å, c = 5.899 Å)

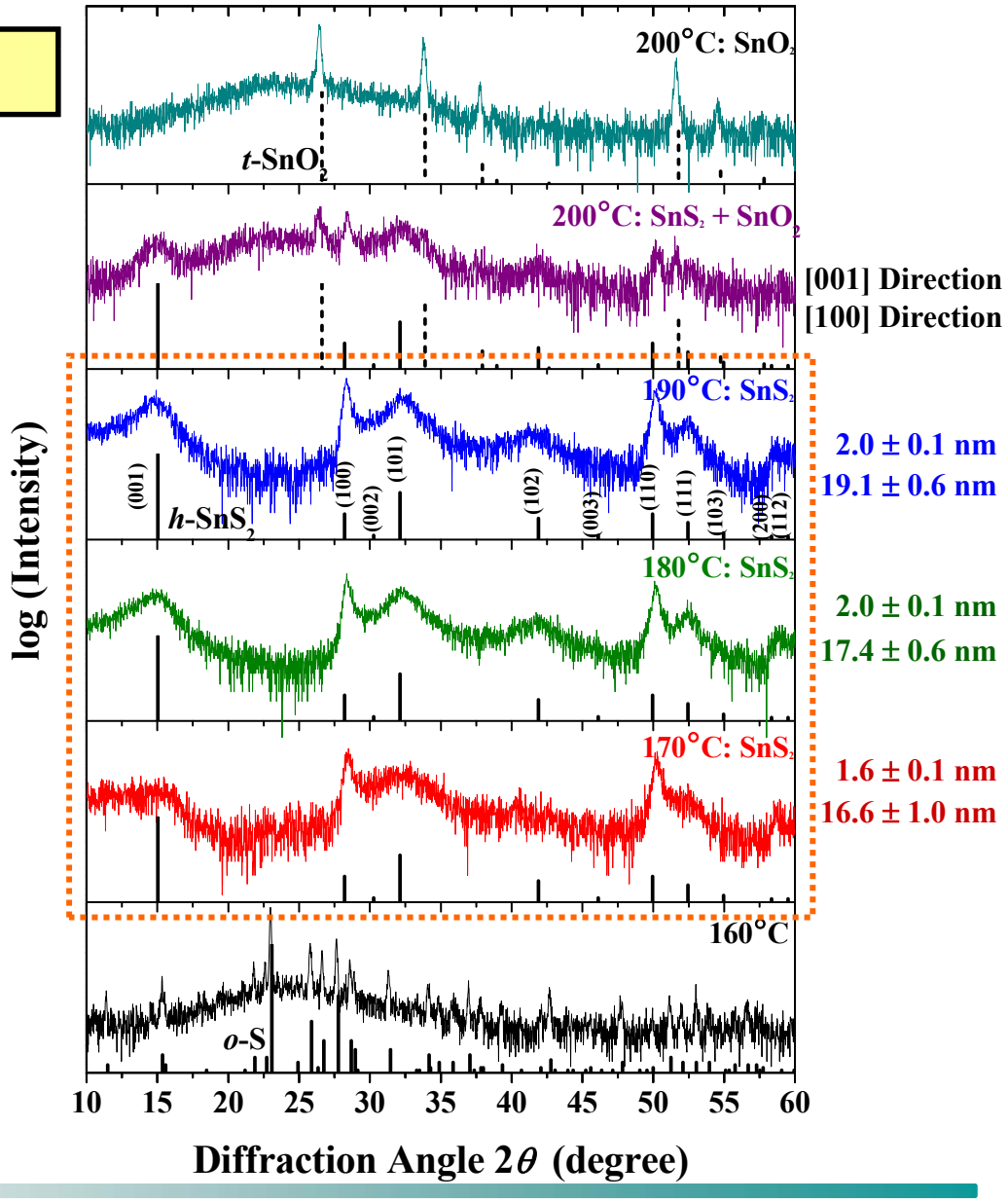

TEM Images of SnS_2 Nanosheets

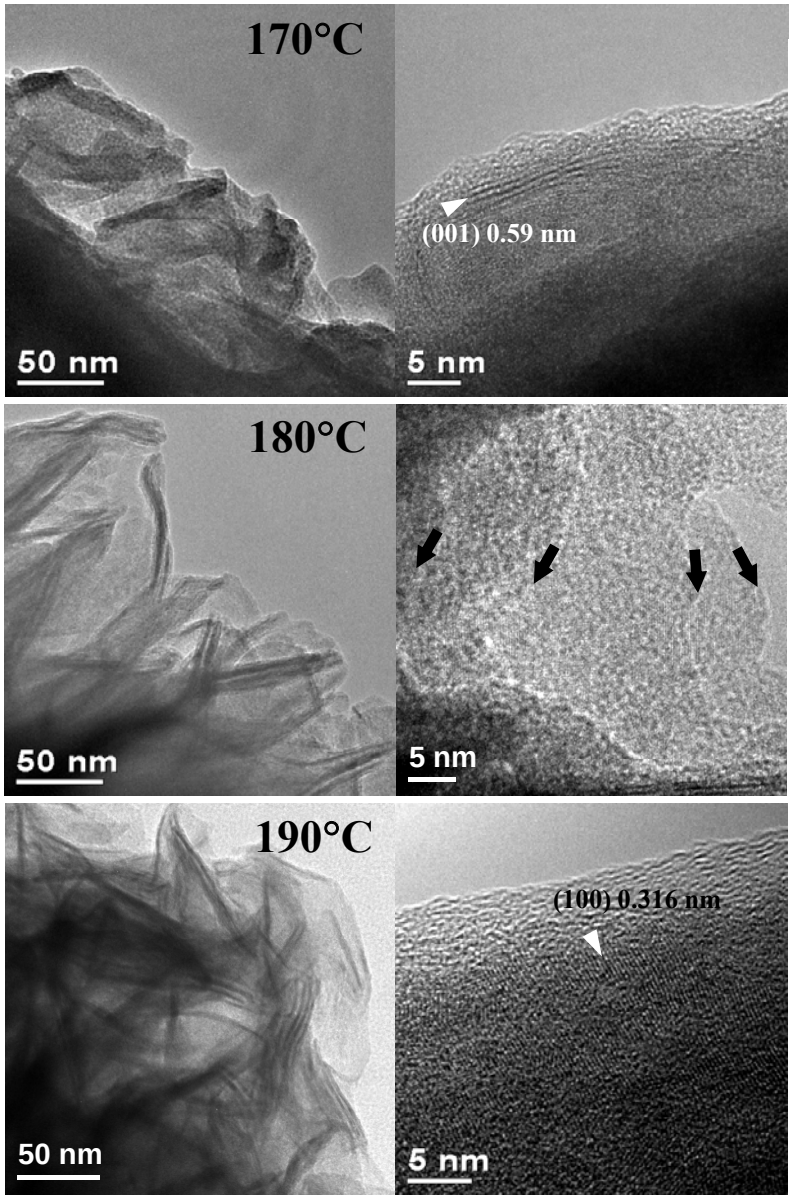

Short Stumpy Flakes

Long Layer-Rolled and Wiggled Sheets

Charge-Discharge Experiments

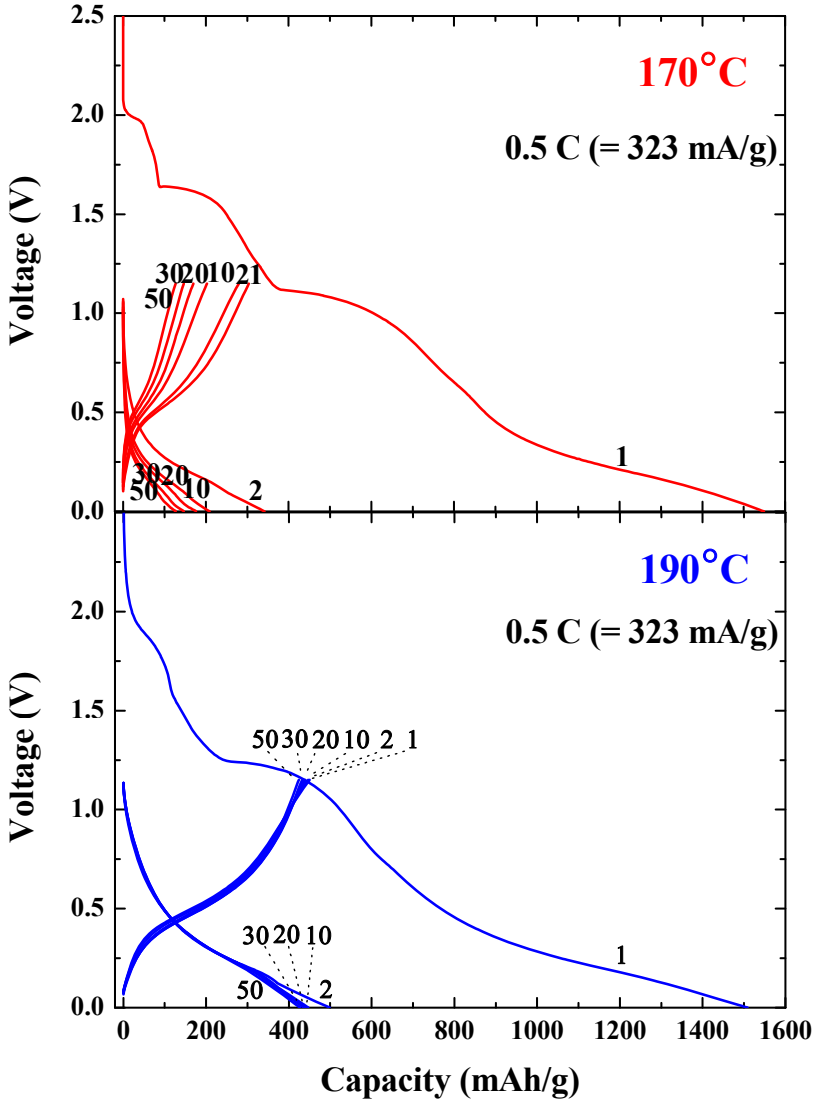

Electrochemical Cycling Test

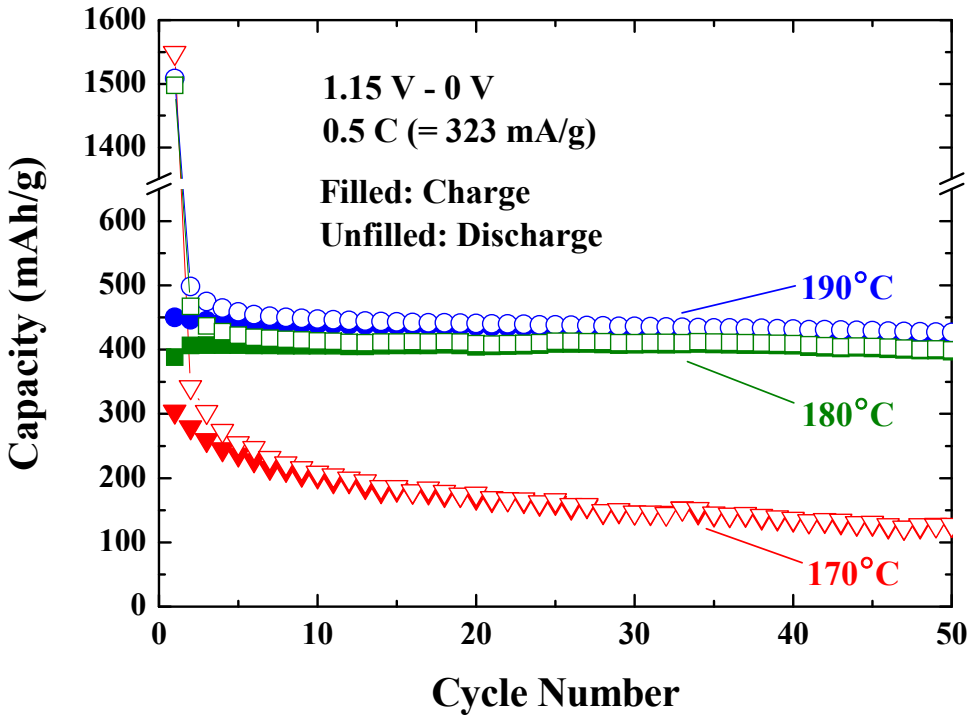

SnS_2-nanosheet anodes synthesized at 180°C and 190°C exhibit excellent capacity retention.

Size Variation of SnS_2 Nanosheets

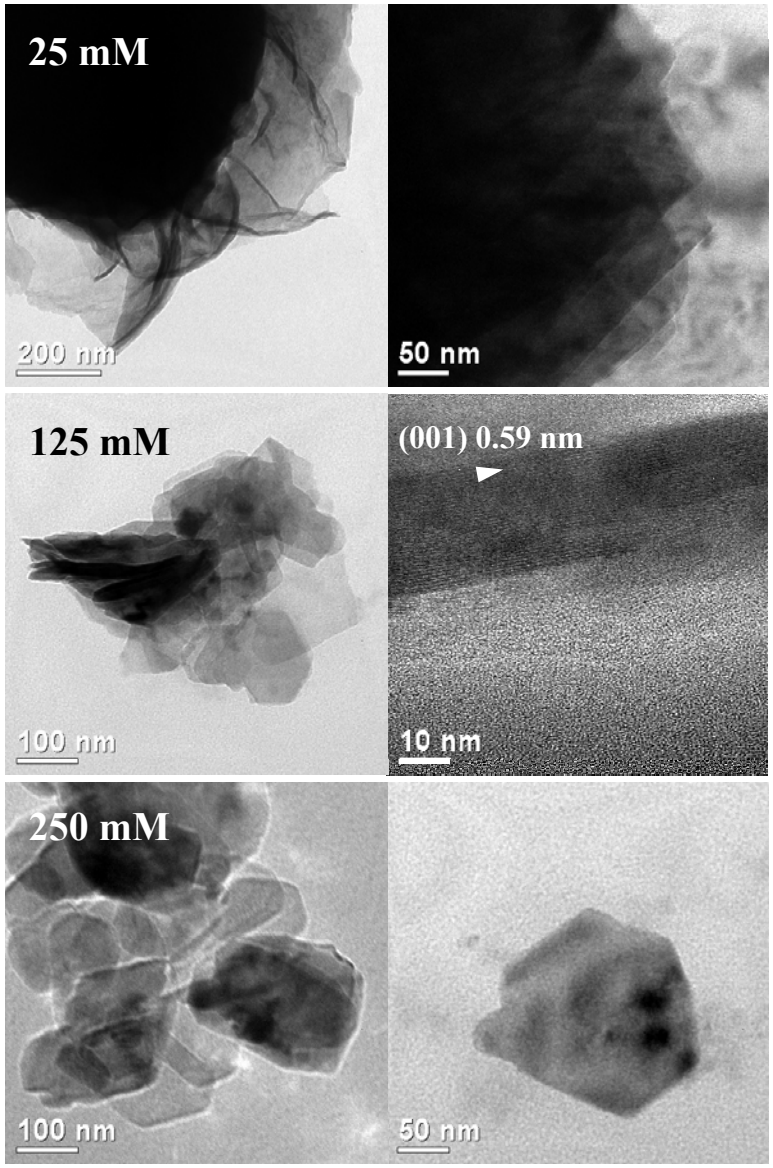

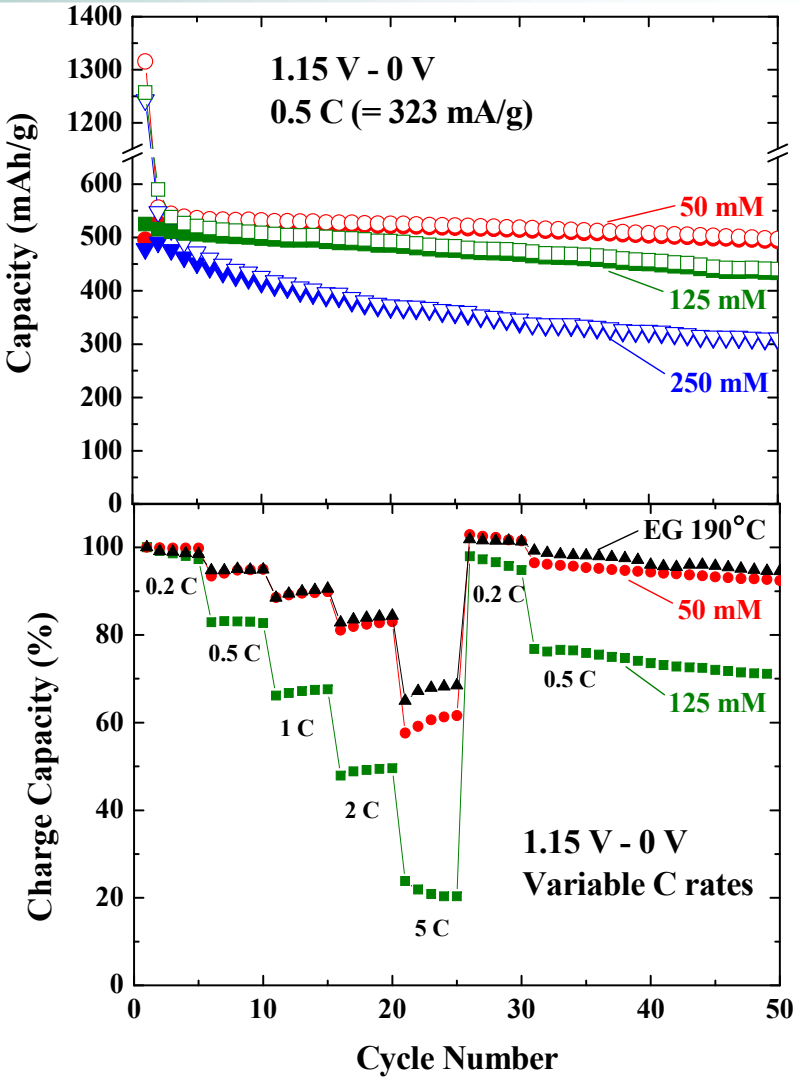

Nanosheets with a smaller thickness show improved electrochemical properties.

WS_2 Nanosheets

Synthesis by J. Cheon's Group

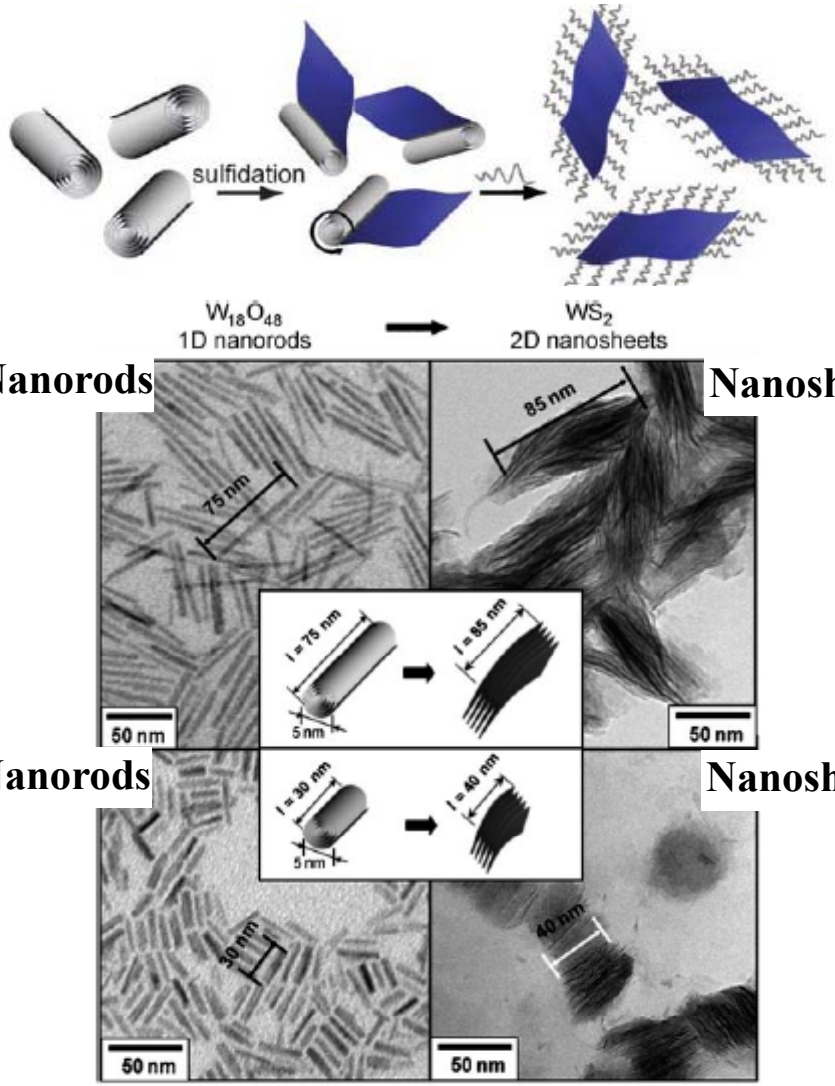

Electrochemical Tests

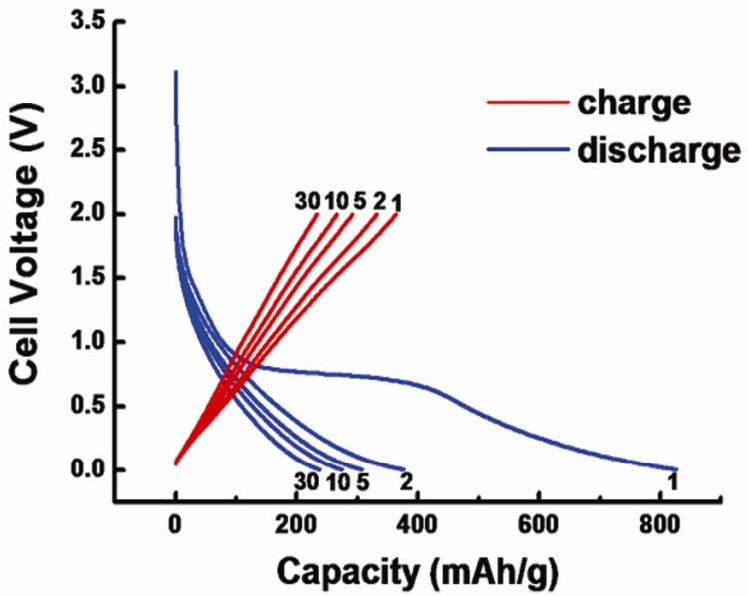

Various Nanostructures for High-Capacity Anode

- J.-W. Seo, Y.-W. Jun, S.-W. Park, H. Nah, T. Moon, B. Park, J.-G. Kim, Y. J. Kim, and J. Cheon *Angew. Chem. Int. Ed.* **46**, 8828 (2007).

Two-Dimensional SnS_2 Nanoplates

Synthesis by J. Cheon's Group

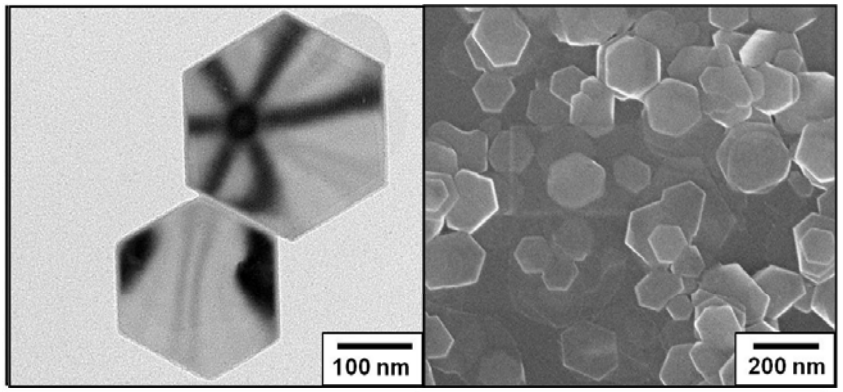

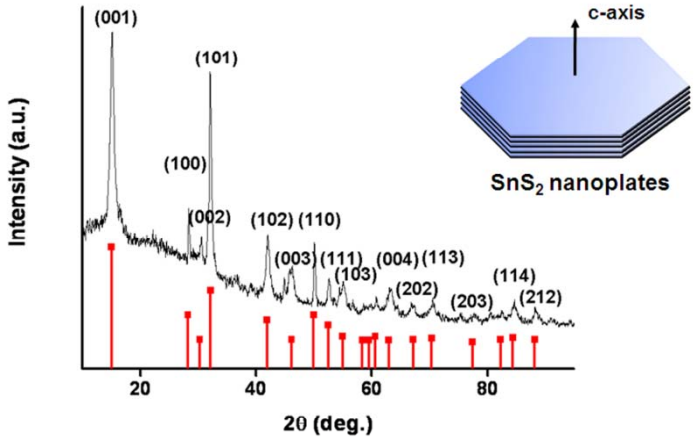

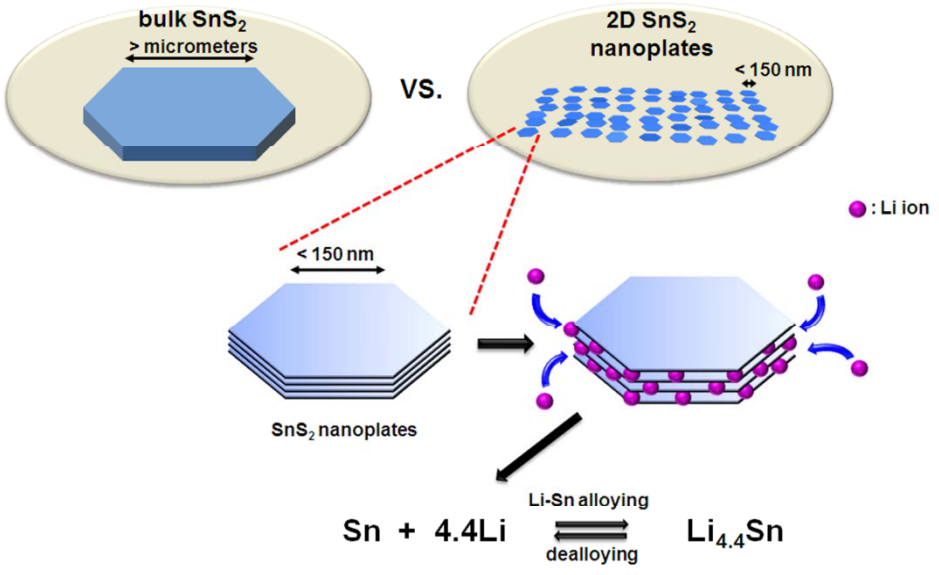

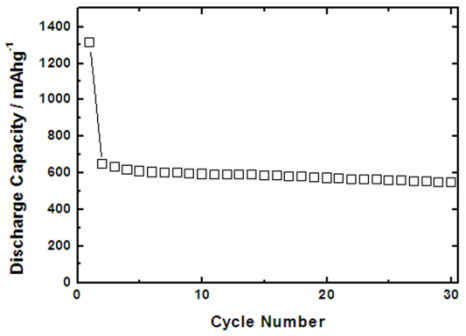

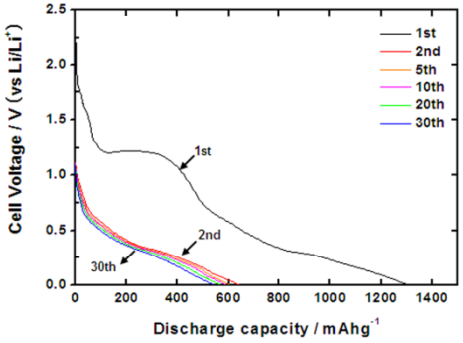

Enhanced electrochemical properties by 2-D layered SnS_2 nanoplates.

- J.-W. Seo, J.-T. Jang, S.-W. Park, C. Kim, B. Park, and J. Cheon *Adv. Mater.* **20**, 4269 (2008).

Nanoscale Interface Control

- Compositions?
- Nanostructures?
- Mechanisms?

http://bp.snu.ac.kr

What is Your Goal for ~80 Years ???